NAVAL POSTGRADUATE SCHOOL

MONTEREY, CALIFORNIA

THESIS

A COMPUTER SIMULATION MODEL OF FLUID FLOW THROUGH A CHANNEL WITH CONSTRICTION

by

William T. Dean

June 2013

Thesis Advisor: Bruce Denardo
Co-Advisors: Gamani Karunasiri
Scott Denardo

THIS PAGE INTENTIONALLY LEFT BLANK

REPORT DOCUMENTATION PAGE			Form Approved OMB No. 0704-0188

1. AGENCY USE ONLY *(Leave blank)*	2. REPORT DATE	3. REPORT TYPE AND DATES COVERED
	June 2013	Master's Thesis

4. TITLE AND SUBTITLE	5. FUNDING NUMBERS
A COMPUTER SIMULATION MODEL OF FLUID FLOW THROUGH A CHANNEL WITH CONSTRICTION	
6. AUTHOR(S) William T. Dean	
7. PERFORMING ORGANIZATION NAME(S) AND ADDRESS(ES) Naval Postgraduate School Monterey, CA 93943-5000	**8. PERFORMING ORGANIZATION REPORT NUMBER**
9. SPONSORING /MONITORING AGENCY NAME(S) AND ADDRESS(ES) N/A	**10. SPONSORING/MONITORING AGENCY REPORT NUMBER**

11. SUPPLEMENTARY NOTES The views expressed in this thesis are those of the author and do not reflect the official policy or position of the Department of Defense or the U.S. Government. IRB Protocol number ____N/A____.

12a. DISTRIBUTION / AVAILABILITY STATEMENT	12b. DISTRIBUTION CODE
Approved for public release; distribution is unlimited	

13. ABSTRACT (maximum 200 words)

Computer simulation is a valuable tool for the research of physics. These simulations can be especially valuable when there is experimental data available that can be used to validate the model. The main objective of this thesis is to determine whether a computer simulation model can accurately depict the experimentally determined fluid flow for a channel with a series of unique individual constrictions. The experimental data are derived from a scaled-up model of coronary blood flow with localized axisymmetric constrictions (or stenoses), representing an ideal case of atherosclerotic disease. This thesis provides the foundation for future study and simulation to develop a microelectromechanical device mounted on a stent capable of sensing and transmitting changes in blood flow characteristics and properties to an outside receiver for improved treatment of patients with atherosclerotic coronary artery disease.

14. SUBJECT TERMS COMSOL, Stenosis, Fluid Dynamics, Hemodynamics	15. NUMBER OF PAGES 67
	16. PRICE CODE

17. SECURITY CLASSIFICATION OF REPORT	18. SECURITY CLASSIFICATION OF THIS PAGE	19. SECURITY CLASSIFICATION OF ABSTRACT	20. LIMITATION OF ABSTRACT
Unclassified	Unclassified	Unclassified	UU

NSN 7540-01-280-5500 Standard Form 298 (Rev. 2-89)
Prescribed by ANSI Std. 239-18

THIS PAGE INTENTIONALLY LEFT BLANK

Approved for public release; distribution is unlimited

A COMPUTER SIMULATION MODEL OF FLUID FLOW THROUGH A CHANNEL WITH CONSTRICTION

William T. Dean
Lieutenant, United States Navy
B.S., United States Naval Academy, 2005

Submitted in partial fulfillment of the
requirements for the degree of

MASTER OF SCIENCE IN APPLIED PHYSICS

from the

NAVAL POSTGRADUATE SCHOOL
June 2013

Author: William T. Dean

Approved by: Bruce Denardo
Thesis Advisor

Gamani Karunasiri
Thesis Co-Advisor

Scott Denardo
Thesis Co-Advisor

Andres Larraza
Chair, Department of Applied Physics

THIS PAGE INTENTIONALLY LEFT BLANK

ABSTRACT

Computer simulation is a valuable tool for the research of physics. These simulations can be especially valuable when there is experimental data available that can be used to validate the model. The main objective of this thesis is to determine whether a computer simulation model can accurately depict the experimentally determined fluid flow for a channel with a series of unique individual constrictions. The experimental data are derived from a scaled-up model of coronary blood flow with localized axisymmetric constrictions (or stenoses), representing an ideal case of atherosclerotic disease. This thesis provides the foundation for future study and simulation to develop a microelectromechanical device mounted on a stent capable of sensing and transmitting changes in blood flow characteristics and properties to an outside receiver for improved treatment of patients with atherosclerotic coronary artery disease.

THIS PAGE INTENTIONALLY LEFT BLANK

TABLE OF CONTENTS

THIS PAGE INTENTIONALLY LEFT BLANK

LIST OF FIGURES

ACKNOWLEDGMENTS

I would like to thank my three co-advisors in the completion of this thesis:

Dr. Bruce Denardo, for organizing the personnel and ideas, as well as providing direction for this multi-faceted endeavor.

Dr. Gamani Karunasiri, for his keen physical insights to complex problems as well as his wealth of assistance with analyzing simulation data.

Dr. Scott Denardo, for his subject matter expertise in all things cardiovascular and his commitment of time outside of his medical practice.

I would also like to thank Dr. John Dunec of COMSOL multiphysics for helping to develop our model and to help us get our ideas into model form. Finally, I would like to thank my wife, Laura, for her patience and assistance during these past several months.

THIS PAGE INTENTIONALLY LEFT BLANK

I. INTRODUCTION

A. BACKGROUND

Despite advances in prevention, pharmacotherapy and revascularization, atherosclerotic coronary artery disease (CAD) remains the leading cause of death in adults (World Health Organization, 2013). The disease typically becomes clinically apparent as remodeling of the artery occurs, including obstruction of the lumen or, in engineering terms, constriction of the channel. Stents are metal scaffolds used in the treatment of CAD. They were first approved by the FDA in 1994 as an improvement over other contemporary catheter-based (i.e., percutaneous) technologies (e.g., conventional balloon angioplasty) and have indeed reduced the principal problems associated with those technologies: abrupt shut-down shortly after the procedure (i.e., sudden re-occlusion, usually consisting of a combination of dissection/tear of the artery wall, spasm and thrombus/clot formation); and the more chronic restenosis (i.e., re-narrowing), which can occur over several months' time.

Unfortunately, stents have two principal limitations that parallel those associated with other percutaneous technologies: (1) thrombosis (0.5–1.5% chance of occurrence during first year after placement); and (2) restenosis (depending upon patient population, artery characteristics and stent design, 5-30% chance of occurrence during first year (DeMaria et al., 2011). Usually stent thrombosis is clinically obvious ("heart attack") and requires emergency percutaneous treatment. However, stent restenosis can be more difficult to diagnose, and frequently requires non-invasive testing and/or repeat cardiac catheterization for definitive diagnosis and to direct further treatment.

Most non-invasive tests designed to monitor for restenosis are active and depend upon the consequent limitation in the flow of blood in the affected coronary artery (Garg, and Serruys, 2010). However, these tests (and cardiac catheterization) can be time consuming, use expensive resources and carry a small but non-trivial risk for causing a life-threatening complication (0.1%). Thus, an inexpensive, passive, non-invasive means for determining blood flow within the coronary arteries following stent placement would,

provide a convenient, timely and safe analysis of conditions within the stent and prove valuable for the patient's cardiovascular care.

The possibility exists for remote sensing from within the lumen to determine blood flow characteristics via a microelectromechanical system (MEMS) device. In principle, a MEMS device that is attached to an arterial stent could utilize the non-uniform flow of blood within the human body to detect changes in pressure. Such changes in pressure could be remotely queried via a radiative energy source (acoustic, electrical, magnetic) in order to provide nearly instantaneous data. The MEMS device would be attached directly to, and installed concurrently with the arterial stent. Such a device would have four principle components: a sensor, a transmitter, a receiver, and a power supply.

The sensor would take direct, real time measurement of blood flow data through a pressure transducer or similar device. The non-uniform nature of blood flow would provide for a measurable pressure difference between the pressure maximum (systolic pressure) and minimum (diastolic pressure). This transducer would measure the quantitative differences in pressure over time and could be compared with previous patient data to provide the medical practitioner a measureable sense of stent effectiveness without necessitating non-invasive tests or cardiac catheterization.

A second possible approach to measuring flow characteristics from within the artery would be to utilize the charge separation in blood flow rather than mechanical pressure. While it is very unlikely that there is a net electric charge generated by blood flow, there is a possibility that there is a charge separation distribution within the lumen. The net electromagnetic force between charged elements remains attractive during the flow, even though the magnetic force is repulsive. Thus, any interaction with the vessel wall must be greater than the electromagnetic force if separation is to be maintained and therefore a distribution of charge density.

As a result, charge separation in blood flow can be utilized for electromagnetic, vice mechanical transduction. For example, the pulsatile nature of the flow can induce a voltage in a loop of wire through which a fraction of the blood flows. This in turn would

provide a measureable voltage capable of comparison with previous, post-procedure data. This data could be used to quantify restenosis.

Human tissue presents a unique challenge to the transmission and reception of traditional radiofrequency signals. Much of this is due to the highly heterogeneous makeup of the human body between separate tissues as well as bone. Possible transmission methods include the use of microwave radiation, acoustic radiation, near infrared radiation, and magnetic resonance imaging.

The unique architecture of the human artery almost certainly dictates that a power source for a MEMS sensor and transmitter will have to be co-located with the stent itself. An external power source located remotely from the sensor/transmitter structure is not feasible, as in the case of a pacemaker. The arterial walls must be left intact in order to help assure vessel integrity and reduce the risk of lumen weakening and a subsequent possibility of aneurysm. Therefore, power must either be supplied via an external man-made source (as in the case of Magnetic Resonance Imaging [MRI]), or from the flow of the blood itself through a MEMS energy harvesting system.

A common investigation in the sensor aspect of such a device is the "stentenna" a device that utilizes the fundamentals of electromagnetic theory (Keikhosravy et al., 2012). The device essentially operates on an LC tank that drives a signal through an antenna that is intrinsic to the metal framework on the stent itself.

Takhata, Gianchandani, and Wise (2006) have investigated such a device. Their proposal is based on the principle that when liquid flows through a channel, there exists a pressure differential due to the difference of the average flow velocity at two discrete locations. Two capacitive pressure sensors are placed in a mock artery, one upstream from a blockage and another downstream. The decrease in pressure from the upstream to the downstream, as well as the separate number of turns for each inductor, provides separate and theoretically discrete signals.

The MEMS field has also produced investigations into flow sensing devices. Aiyar, Song, Kim, and Allen (2009) have made investigations into an airflow sensing MEMS device used to detect flow changes across the wings of unmanned aerial

vehicles. Their experiments yielded a cantilever type MEMS device capable to detecting small changes in airflow characteristics. Such devices are small enough as to not interfere with the aerodynamic performance of smaller, unmanned aerial vehicles. This is a very important consideration when introducing some sort of flow detection within a human artery.

B. APPROACH

The complexity of such a MEMS device placed within the human vascular system presents myriad challenges toward its timely development and implementation. Advances in computer software programs dealing with physical systems offer an approach capable of expediting device development without the time and expense associated with traditional prototype development. In the case of the human vascular system, such simulation software would be invaluable in identifying the effects of device implantation as well as identifying process errors between the blood/device interface.

While computer simulation does provide great flexibility in its approach toward solving complex physical problems, it must be ensured that these simulations accurately portray the true nature of what is actually happening. Before such a device can be developed for simulation, the software itself must be validated. Comparison of known experimental data against a selected simulation program is the foundation for future design and development considerations in a cardiovascular MEMS device.

Denardo, et al.(1990) developed an experimental scaled-up model of blood flow through a constricted channel and used laser Doppler velocimetry (LDV) to measure velocity profiles upstream, within and downstream from a series of constrictions. Although the stimulus for development of that experimental model was to correlate flow disturbances caused by the constrictions with changes in simultaneously acquired Doppler data using a scaled-up Doppler catheter, the LDV experimental data are still available for use in other contexts.

The multiphysics software COMSOL was selected as the candidate for comparing this known experimental data with simulation. COMSOL was selected due to its versatility in addressing physical simulations across a wide spectrum of scientific fields

and disciplines thus enabling compatibility between the computational fluid dynamics field and the microelectromechanical field. With that potential compatibility in mind, it must be determined that COMSOL can reasonably simulate and replicate the aforementioned experimental data accurately.

Validation of the computer model could assist in leading to future design, development, and understanding of biologically implanted MEMS device, provided that such simulations accurately reflect known experimental data. The capability for COMSOL to interface multiple physical disciplines would provide for a more seamless approach to future developments on a microscale.

This thesis will describe the setup of the previous experimental work conducted by Denardo et al. (1990), the computer simulation model and its associated assumptions, and the comparison of results to experimental data. The comparison of experimental and simulated data, as well as their implication, will determine the requirements and course of future research and study for a functional MEMS stent monitoring system

THIS PAGE INTENTIONALLY LEFT BLANK

II. PREVIOUS WORK

To physically explore the fluid dynamic effect of a constriction to coronary blood flow, an *in vitro* experiment was conducted by Denardo et al. (1990) using a scaled-up model of a coronary artery with stenoses in the range 20-90% cross sectional area (Figure 1). The flow was set at Reynolds numbers representative of coronary blood flow (range, 200-400 ±5%). All experimental setups were conducted with and without a central annulus running through the center of the artery to simulate the effect of a guidewire during angioplasty and stent procedures.

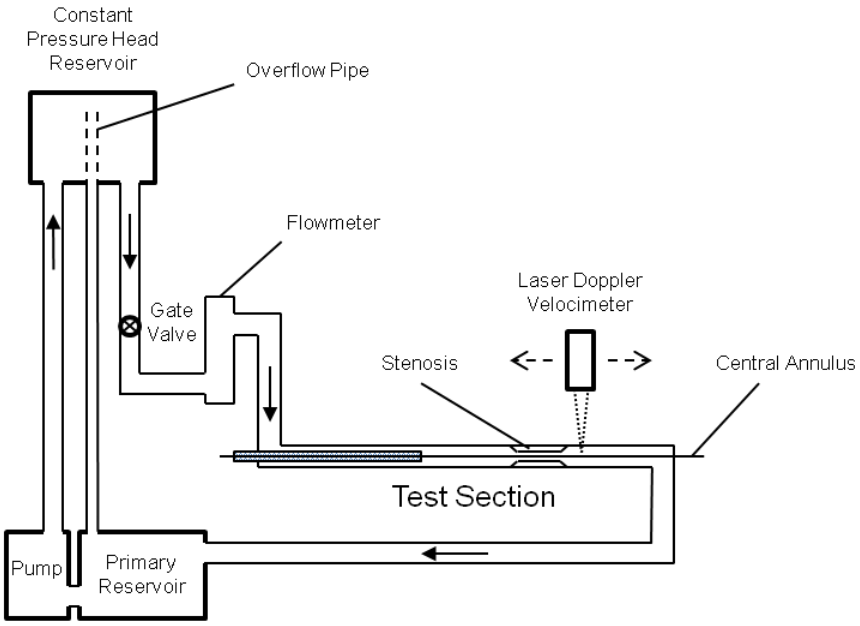

Figure 1. Experiment setup showing scaled up artery with stenosis and guidewire. (After Denardo, 1990)

The model test section was constructed from a straight acrylic tube (internal diameter, 2.54 cm). Acrylic was selected for the test section due to its optical clarity, so that fluid dynamic measurements could be taken using a laser-Doppler velocimeter (LDV). In order to ensure fully developed, laminar flow and to avoid entry effects, the test section length was 133 cm. The constant pressure head reservoir of the model was designed to deliver continuous flow of fluid at a constant perfusion pressure to the gate

valve as measured by a mechanical flowmeter. The height of the fluid in the upper reservoir was maintained at a constant level by means of an overflow pipe. The gate valve was adjusted in order to throttle the mass flow rate in order to adjust and set the desired Reynolds number.

The test fluid used in the model was a mixture of distilled water and glycerol. Because the ratio of water and glycerol changed over time, the index of refraction of the test fluid was determined prior to LDV data collection and characteristics of the fluid (e.g., density, specific gravity, viscosity) were determined using standard tables. The changing nature of the glycerol and water combination necessitated a periodic recalibration of the flowmeter to determine the correct mass flow rate consistent with the Reynolds number desired.

The test section was approximately 133 cm downstream from the last turning point in the system, to ensure fully developed flow entering each constriction. Each constriction, symmetrically machined from an acrylic rod, was placed in the test section and LDV data were acquired at axial positions proximal, at and distal to the center of each constriction. The range of cross sectional areas for the constrictions simulated a range seen in clinical practice. The constrictions had an outside axial length of 2 tube diameters (5.08 cm) and the angle between the inner wall of the tube and the angled face of the stenosis was 45 degrees. The variations between the individual stenoses arose from the difference in depth from the inner wall of the tube and the axial length at the inside of the stenosis.

LDV data were collected at 9 axial positions for each constriction, at 1.00 mm radial increments, and for each of the three Reynolds numbers 200, 300, and 400. The specific constrictions, by cross sectional area, were: 20%, 30%, 40%, 60%, 75% and 90%. For each constriction, LDV data were acquired with and without a central annulus representing a guidewire. This central annulus was a stainless steel rod 0.5 cm in outer diameter painted flat black in order to reduce any reflective interference on LDV measurements. Initial conditions were calculated according to Reynolds number for laminar flow within a cylinder and are given by

$$\mathrm{Re} = \frac{\rho \cdot \mathrm{v} \cdot \mathrm{D}}{\mu} \quad , \tag{1}$$

where Re is equal to the dimensionless Reynolds number, ρ is the density of the test fluid in kg/m^3, v is the average velocity in m/s, D is the test section inside diameter in m, and μ is the dynamic viscosity in Pa·s.

The 9 axial locations for LDV data acquisition were relative to the axial center of each constriction. The first two axial positions were upstream, by 1.500D and 1.000D. The next three positions were from within each constriction: 0.475D upstream, at the axial center (0.000D) and 0.475D downstream. The remaining four positions were downstream, by 1.000D, 1.500D, 2.000D and 2.500D. The reason for taking more measurements downstream versus upstream was to more carefully study the regions where each constriction was presumed to have a greater fluid dynamic effect, presuming the upstream flow condition would closely resembled that of standard Hagen-Poiseuille flow in a cylinder:

$$u(r) = u_{\max} \cdot (1 - \frac{r^2}{R^2}), \tag{2}$$

where r is the radius from the center of the duct in m, u_{max} is the maximum axial velocity at the center of the duct in m/s, R is the overall internal radius in m, and u(r) is the velocity at any given r in m/s. This equation assumes laminar flow with a no slip boundary condition.

The LDV system consisted of a 1.5 W argon laser with single color mode wavelength of 514.5 nm (Lexus Model 85, Palo Alto, CA), a beam splitter with appropriate transmitting and receiving optics (TSI Models 915 and 918 respectively, Minneapolis, MN), and a photomultiplier tube with DC power supply (RCA Model 4526, Somerville, NJ; Hewlett Packard Model 51 15A, Palo Alto, CA, respectively). A system of mirrors was used to guide the laser beam from the laser into the beam splitter, and the pinhole diameter of the photomultiplier tube was 0.203mm. Real-time online data analysis of the photomultiplier output was performed using a signal processor (TSI Model 550 "Intelligent Flow Analyzer"). The collecting optics were positioned 19.0 cm from the sample volume which had dimensions 0.32 x 0.16 x 0.16 mm^3. Net radial position error of the setup was ± 0.15 mm (Denardo, 1994).

THIS PAGE INTENTIONALLY LEFT BLANK

III. COMPUTER MODEL

The development of a microelectromechanical System (MEMS) device for use in the human body first requires an effective simulation model to understand the blood flow. The complexities of the human body, the nature of blood flow itself and the microscale of the operating environment produce many challenges. Therefore, validation of COMSOL compared with data from the scaled-up model would provide valuable insight as to whether or not computer simulations truly capture the nature of the flow inside of an arterial system. The COMSOL software provides a wide range of applications to many areas of study in the physical sciences. The capacity to process both MEMS and fluid mechanics simulations became the determining factor in proceeding with COMSOL.

Before proceeding with the more complex aspects of the problem, it was necessary to confirm that COMSOL could adequately process a simpler and more fundamental experiment. Given the wealth of data provided from previous work, in particular from the in vitro scaled up model of coronary flow described above, a comparison and duplication of results seemed to be the most logical choice. An accurate prediction of flow dynamics using COMSOL comparing to the previously acquired experimental data from the scaled-up model would validate the use of COMSOL in future applications for MEMS design in such a system.

To model the in vitro experiment, fluid flow module of COMSOL 4.3a was used. Due to axisymmetric fluid flow employed in the experiment, a two dimensional model was used for the simulation. Within fluid flow module, the single phase laminar flow sub-module was selected due to the laminar nature of the flow from observed experimental data.

The flexibility of the COMSOL program allowed for to-scale reproduction of the experimental environment. The model consisted of an inlet, the evaluated length of acrylic cylinder and an outlet. The inlet served to simulate the section of cylinder immediately downstream from the flowmeter (Figure 1). The inlet within the model served as the primary boundary for modifying flow conditions. The inlet boundary was

placed 2.54 cm inside diameter in order to match the conditions of the in vitro experiment. Locations downstream of this inlet were to be considered in the test section and to be initially evaluated based solely on this upstream boundary condition for comparison to experimental data. Figures 2 and 3 show the entire model geometry as well as a close up view of the entrance of the stenosis.

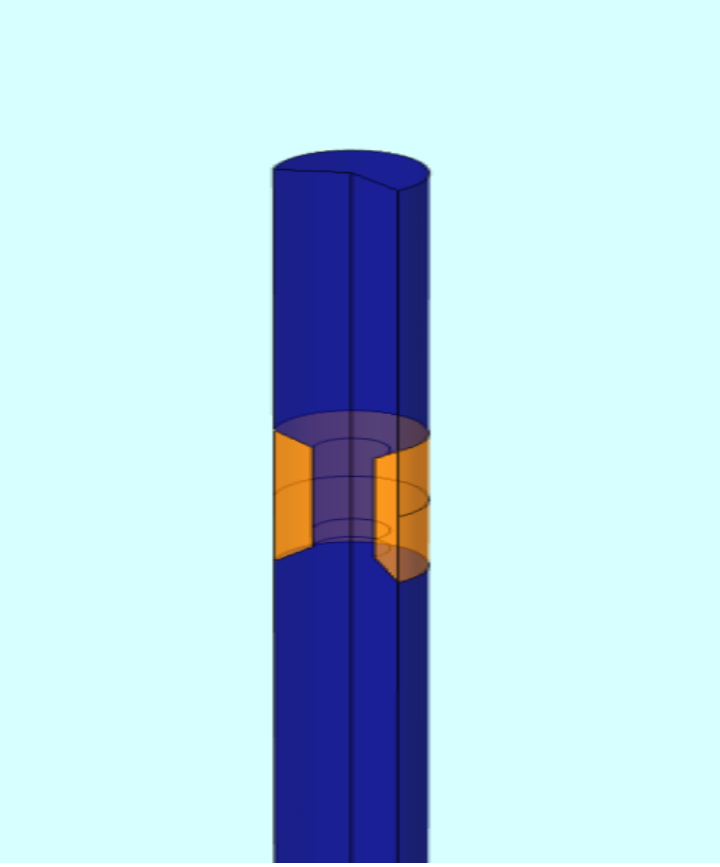

Figure 2. Three-Dimensional rendition of the 75 % stenosis prior to simulation. With the mock artery in blue and the stenosis in gold. The length of the model has been reduced in this case to show greater detail.

.

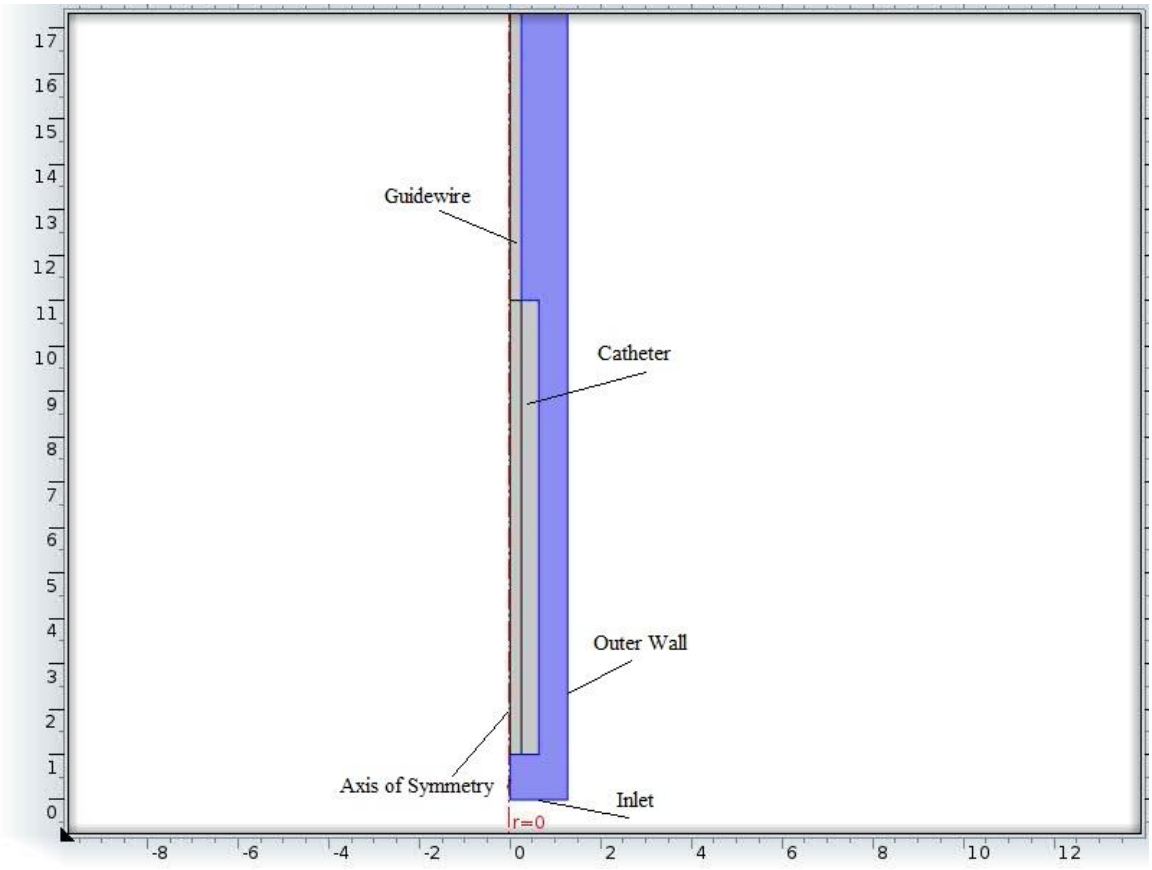

Figure 3. Schematic of the inlet (at bottom center), the catheter with the guidewire housed inside are visible toward the axis of symmetry (left). The units are in centimeters.

Downstream of the inlet, a length of cylinder was added. It was constructed to have sufficient axial distance to ensure that fully developed, parabolic laminar flow occurred prior to arrival within the test section of the model. This cylinder was 80 cm in length from inlet to the test section to allow for the proper flow conditions at the highest analyzed Reynolds number (400). Fully developed flow following entry is determined by Equation (3) and is given by (White, 2003)

$$L = 0.06 \cdot \mathrm{Re} \cdot D, \tag{3}$$

where L is the entrance length for laminar flow inside of a cylinder, Re is the Reynolds number, and D is the diameter of the cylinder. As a result, the longest possible entrance length—for Re 400—required was 61 cm. The longer 80 cm was selected because a

simulated Doppler catheter (outside diameter, 1.27 cm) was placed in the model for other studies not related to this project. The length of 80 cm therefore allowed for a test section that could accommodate both the scaled-up Doppler catheter and still provide the axial distance to allow for a sufficient entrance length for fully developed flow.

The test section is defined as the section of the to-scale model from 1.5 cylinder diameters upstream of the axial center of the stenosis to 2.5 tube diameters downstream of the same stenosis. Because each stenosis, regardless of cross-sectional area, had the same exterior length, this location was the same for all experimental setups. All measurements taken from the simulations were conducted in relation the axial center of the stenosis. In the experiment, each stenosis was machined from an acrylic tube with a trapezoidal geometry (see Figures 4 and 5).

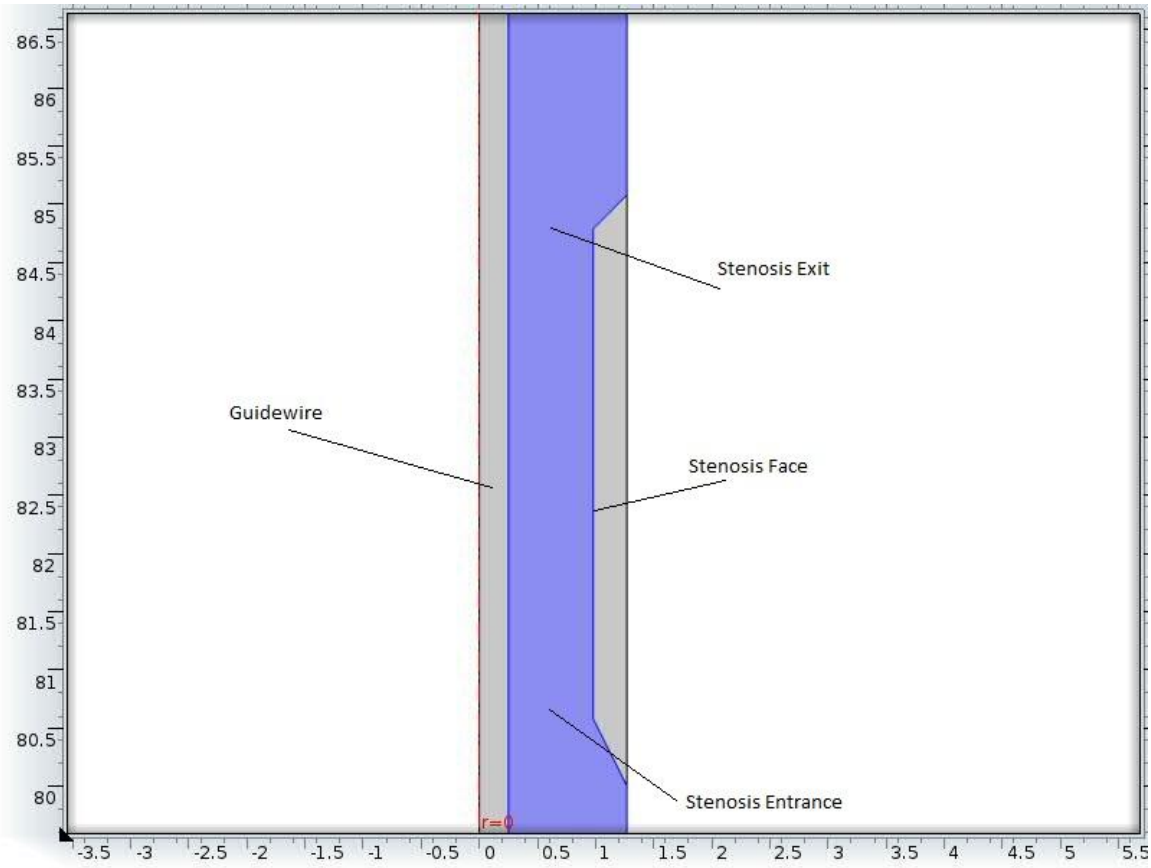

Figure 4. View of the test section of piping. The trapezoidal stenosis is clearly visible at the right. The upstream portion of the flow arrives from the bottom of the picture and the guidewire is present along the axis of symmetry(left). The units are in centimeters.

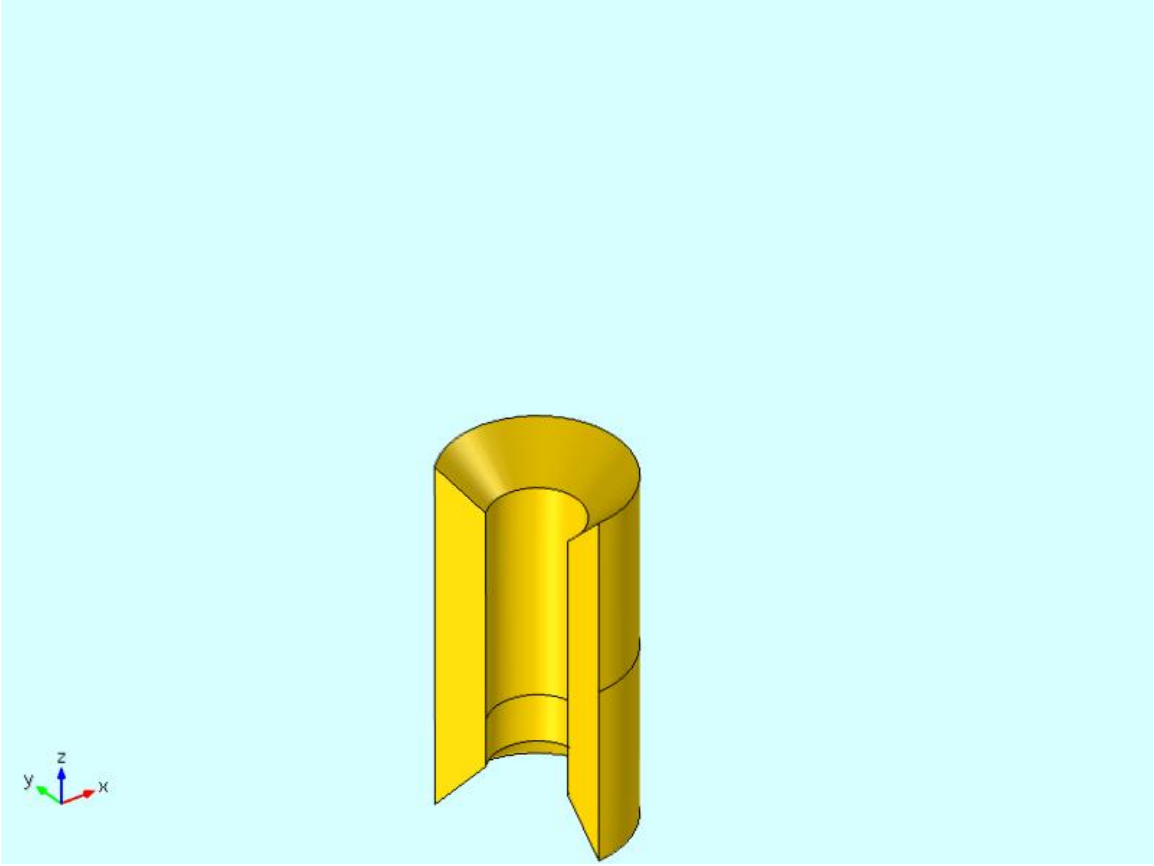

Figure 5. Three dimensional representation of the 75 % stenosis created in the simulation model.

The exterior length of each stenosis was 2 cylinder diameters and each base angle was 45 degrees. The variation in severity of the respective stenoses resulted only in a change of stenosis thickness and the length of the stenosis face. In addition to the stenoses, a central annulus was constructed to run axially down the model from the inlet through the outlet of the system. This central annulus served as an idealized model of a guidewire, as used during angioplasty and stent procedures. The guidewire was assumed to be perfectly straight and exactly in the center of the mock artery and had an outer diameter of 0.5 centimeters. The guidewire was added and removed by enabling/disabling the geometry within the simulation as conditions dictated.

The cylinder composing the test section extended an additional 20 cm beyond the test section to ensure no unexpected fluid dynamic effects at sites of data collection. At the end of the cylinder, an outlet boundary was constructed. No specific boundary

conditions were imposed upon it with the exception of allowing the test fluid to flow through it. This was necessary in order to achieve a steady state condition with an incompressible flow.

COMSOL allows for material selection for each domain in the simulated environment. One may select from a material library from a variety of solids, liquids, and gases or create a new material with manually inputted material parameters dependent on the physics module or modules involved. In the case of this in vitro experiment, the stenoses, guidewire, catheter, and test section walls were assumed to be impermeable. In the case of the laminar flow module, material selection of these boundaries is not necessary, only the properties of the fluid in laminar flow require parameterization.

In the case of the in vitro experiment, the fluid properties changed to a relatively minor degree over time. The liquids were always a mixture of distilled water and glycerol but the volumetric ratios changed following periodic cleaning of the system. Therefore, a new material was created in the module where the density and the dynamic viscosity terms remained variable thus allowing for more flexibility during computation. Within the laminar flow module, the density and dynamic viscosity terms are the only material dependent requisites for steady state flow calculation.

The fluid flow module allows for a wide variety of assumptions about the artificial environment established. In case of this experiment duplication, the laminar flow sub module was determined to be adequate for the parameters involved. Within the laminar flow sub-module, additional assumptions must be made regarding the nature of the flow and the boundary conditions.

The physical module within the laminar flow model used was for incompressible flow. This is largely due to the fluid in question being a combination of glycerol and distilled water on the order of equal amounts of each by volume. Initially, fluid/solid boundaries were assumed to be under the classical no slip condition and were imposed at all boundaries; essentially all velocities at the boundary would be zero. Later developments would reveal that the no-slip condition would not serve to adequately

portray experimental data at all liquid/boundary interfaces, a subject further discussed in the results and comparisons portion of this thesis.

The inlet boundary established the conditions for fluid flow. Given that the experimental data were recorded in terms of Reynolds number and location dependent velocity, the laminar inflow boundary condition was imposed with average velocity and entrance length being the dependent variables in this condition. The average velocity could be calculated either from the Reynolds number or deduced from the experimental data.

Meshing is an important consideration when constructing simulations within COMSOL. The mesh is the relative size of actual elements analyzed while performing finite element modeling (see Figure 6). COMSOL contains a host of separate meshing methods dependent on size and geometry and are adjustable throughout the entire model. Error analysis was conducted within the computer model by adjusting the mesh refinement and comparing results. Within this two-dimensional, axisymmetric model, meshing was assumed to be normal (approximately 15 discrete elements across at the narrowest point) and compared with both the finer and extremely fine mesh resolutions (approximately 25 and 75 discrete elements in the radial direction at the narrowest point respectively). The changes in the mesh resolution yielded no appreciable changes for any of the experimental setups.

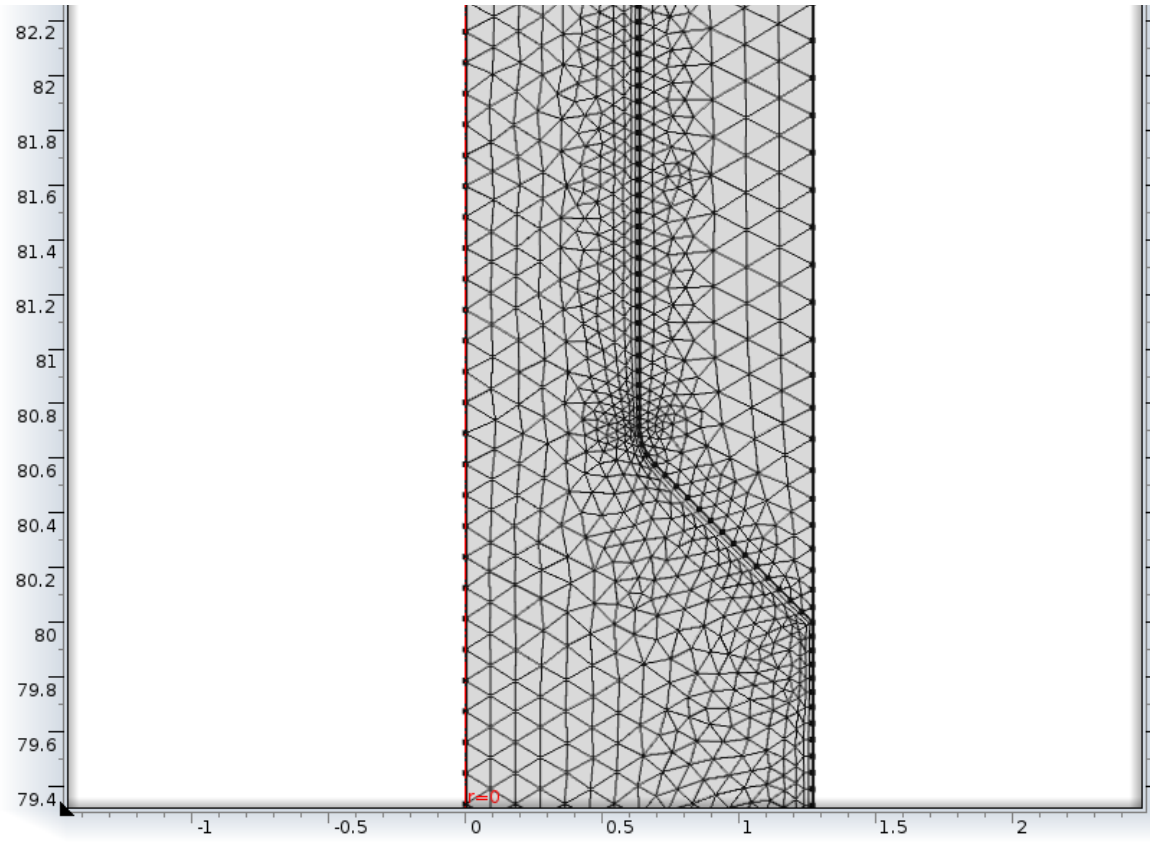

Figure 6. Meshing makeup of the 75 % stenosis without the guidewire. At the vertex alongside the stenosis entrance there is an increase in the density of elements to account for greater physical changes at the entrance of the stenosis.

For determining the solution to each experimental setup, the stationary solver feature was used within the simulation. The stationary solver determines the nature of all parameters once a steady state has been reached. Given that turbulence was not an expected result of these simulation, the stationary solver was deemed adequate for this case. Simulations would later reveal that the stationary solver was not ideal for the highest grade stenoses. Flow separation downstream of the most severe stenosis (90 percent) yielded unsteady, albeit non-turbulent, behavior. This phenomenon will be discussed in greater detail at the results and comparison section of this thesis.

Once solved, each experimental case had its velocity profiles analyzed. Figure 7 shows the simulated velocity profile of a 40% stenosis at 1.5 diameters upstream of stenosis center.

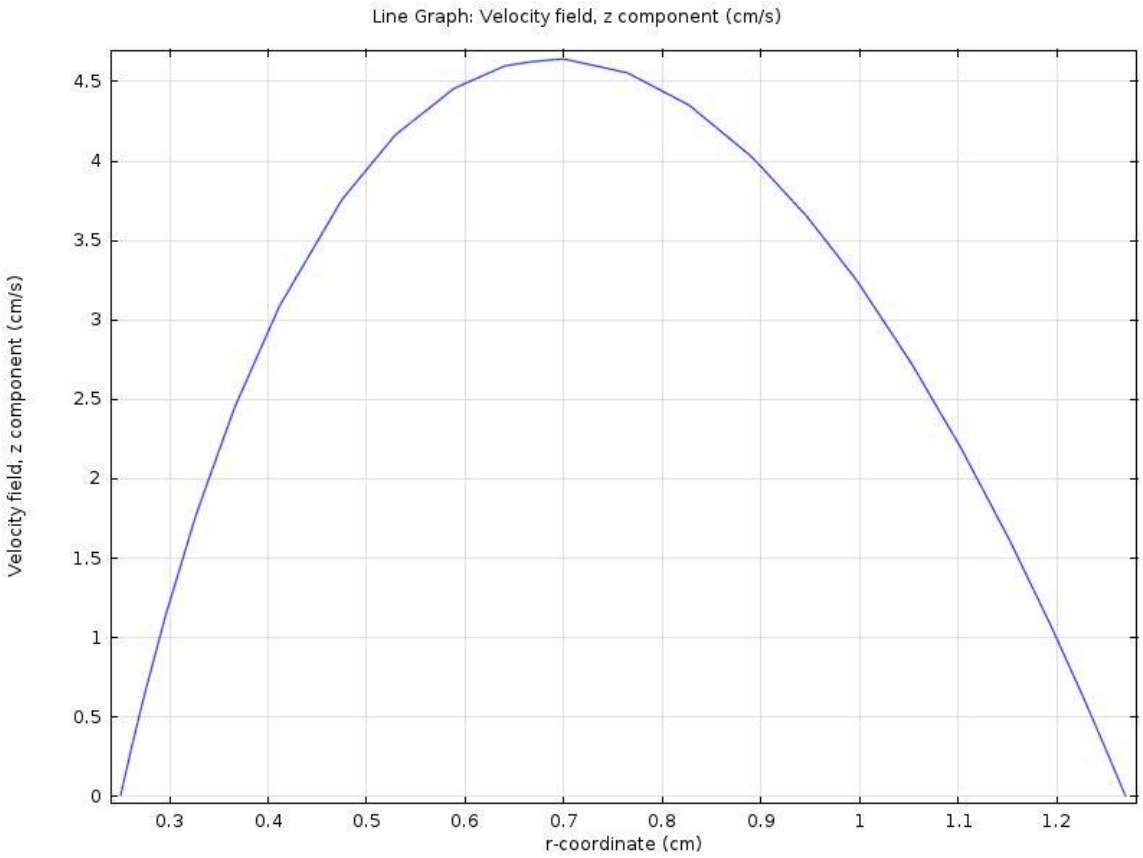

Figure 7. One dimensional plot of the velocity profile 1.5 diameters upstream of stenosis center. In this case, a guidewire is present as denoted by nearly zero velocity profile at 0.25 cm from the axis of symmetry.

Velocity profiles of predetermined axial locations were observed, recorded, and exported from the COMSOL software package as a spreadsheet where the data were then graphed and compared to experimental data. The graphical analysis from COMSOL provided additional information as to the nature of the flow. In particular, it proved useful in identifying areas of recirculation downstream of stenosis center (see Figure 8).

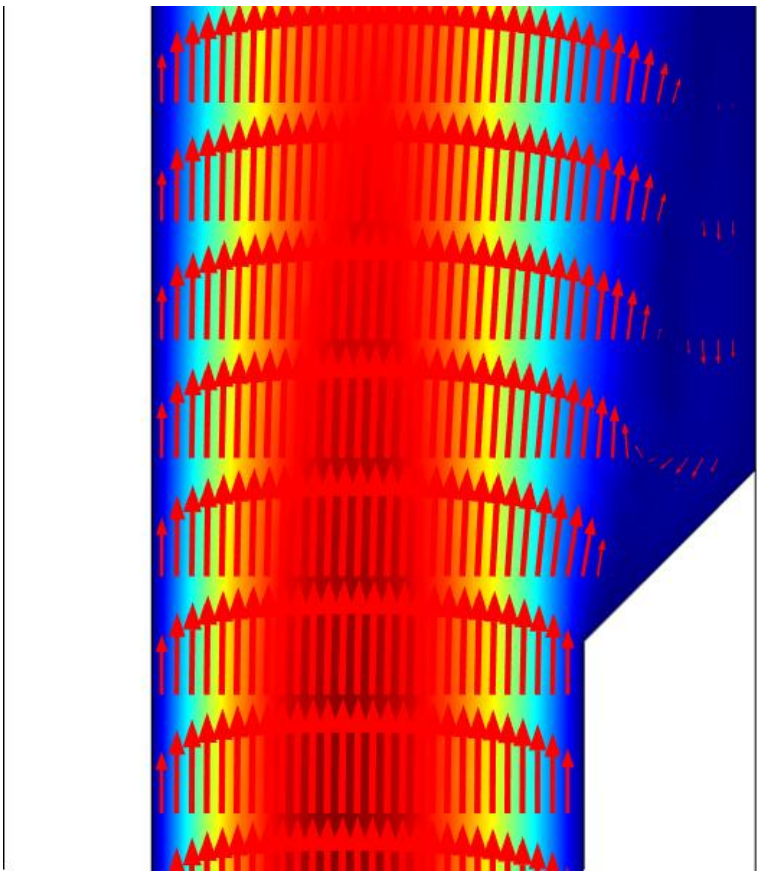

Figure 8. Two dimensional proportional velocity vectors provided from COMSOL multiphysics. Recirculation is clearly visible toward the artery wall, away from the stenosis (right). The guidewire and stenosis are visible in white.

While simulations were run for all experimental Reynolds numbers and configurations, experimental data show a linear relationship between Reynolds number and velocities. The data in Figure 9 show the flow progression of the 75% stenosis without the guidewire normalized so that all Reynolds numbers are equal to 100. The graph clearly shows the aforementioned relationship.

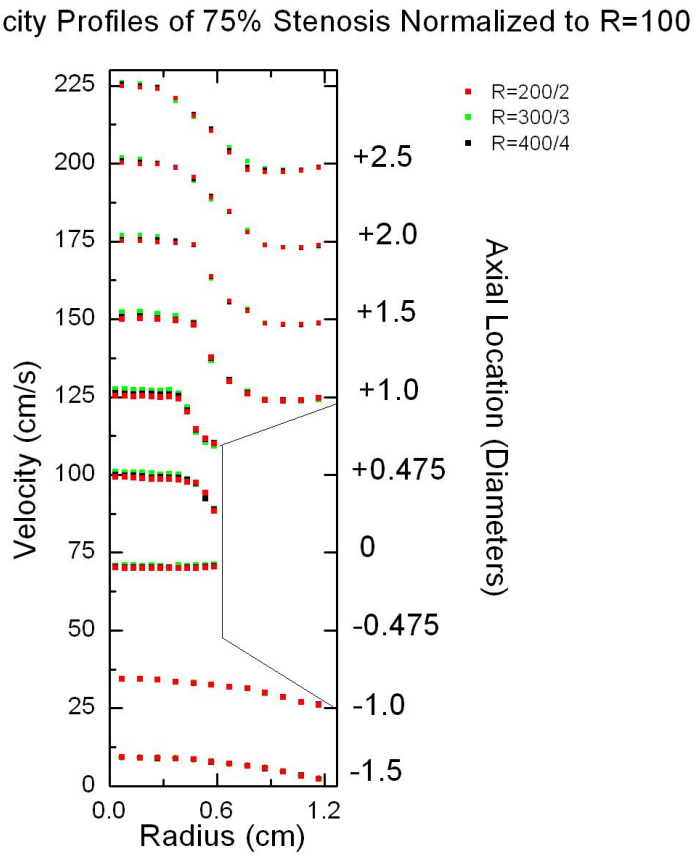

Figure 9. Velocity profiles of experimental data for three different Reynolds numbers (200, 300, and 400) normalized to 100. Each axial location is placed at 25 cm/s intervals so that all data may be viewed at the same time, for instance the data set at the -1.0 axial location has 25 cm/s added. While variation does exist, no particular Reynolds number configuration appears to be dominant in altering the results.

THIS PAGE INTENTIONALLY LEFT BLANK

IV. RESULTS AND COMPARISONS

A. 20% STENOSIS

1. No Guidewire Case

The first experiment analyzed was for the 20 % stenosis (reduction of cross sectional area by 20%). This stenosis was the lowest grade analyzed through experimental means. Identical to all other experimental stenoses, the 20 % stenosis was two tube diameters in outside length and the angle between the tube wall and the stenosis was 45 degrees. Velocity measurements were made using a laser Doppler velocimeter (LDV) at 9 discrete axial locations. The axial locations recorded were in relation to the axial center of the stenosis or the 0D location. Three measurements were taken upstream of the 0D location at 1.500 diameters upstream (-1.5), 1.000 diameters upstream (-1.0), and 0.475 diameters upstream (-0.475). Downstream measurements were taken at 0.475 diameters (+0.475), 1.000 diameter (+1.0), 1.500 diameters (+1.5), 2.000 diameters (+2.0) and 2.500 diameters (+2.5). The purpose for choosing the 0.475 diameters instead of 0.500 diameters was to ensure the ability to acquire LDV data in close proximity of the higher grade stenoses to the 45 degree angled inlet and outlet. Importantly, the 45 degree angle at the inlets and outlets would inappropriately refract the split laser beam and disable LDV data collection.

Radial measurements were obtained relative to the inside surface of the model artery, starting at 1.00 mm (±0.15 mm). Within the stenosis, measurements were taken at the same 1.00 mm intervals measured from the inside surface of the stenosis. This yielded a range of data points from 11.4 mm to 0.4 mm relative to the center of the model artery.

Density and dynamic viscosity were taken from experimental data and inputted into the model. Average velocity was calculated as the maximum velocity divided by two at the center most data point at the -1.5D axial location. This corresponds to the Hagen-Poiseuille [Equation (2)] for laminar flow within a cylinder where no slip exists at the boundary and this value was also inputted into the model. In this case the average velocity calculated was 3.16 cm/s. Results were approximately as predicted and closely

resemble experimental data in terms of both the relative changes in velocity magnitude as well as the general shape of the velocity profiles at each axial location. Figure 10 shows the velocity profiles at each axial location. The velocity profiles within, and directly downstream of the stenosis are increased by approximately 20 % as compared with the velocity profiles upstream of the stenosis as expected via the continuity equation. The results for Reynolds numbers of 300 and 400 show similar results and scale linearly similar to Figure 9. The no slip boundary condition provides an adequate model for this data set as both the experimental and simulated data points tend to zero toward the boundary.

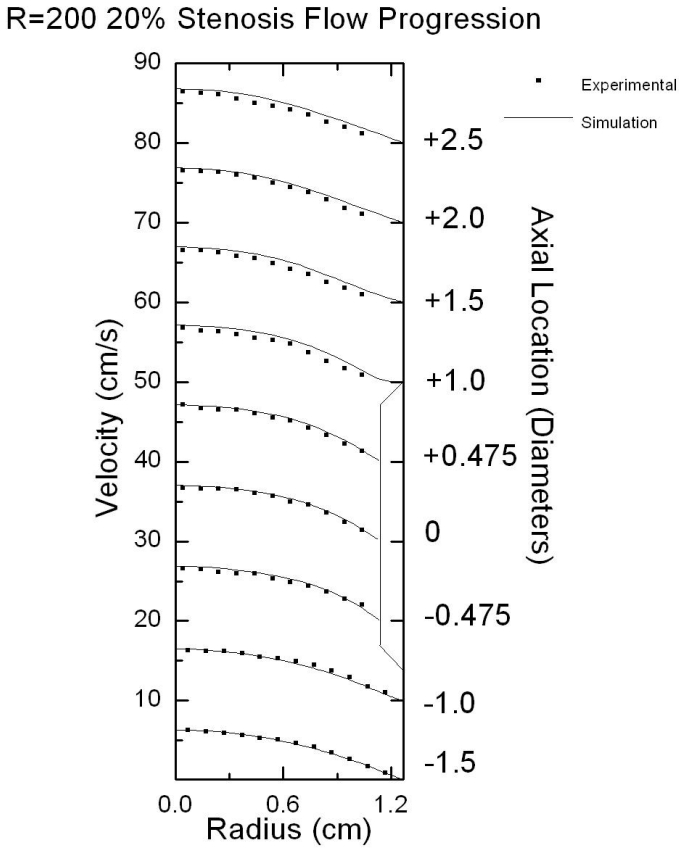

Figure 10. Flow progression of the 20% stenosis. Axial measurements are labeled on the right hand margin and velocity profiles are separated by 10cm/s intervals for greater clarity.

2. Guidewire Case

The 20% stenosis with the guidewire assumes the same initial conditions as the 20% stenosis without the guidewire in terms of density, dynamic viscosity, and initial average velocity. However, experimental data indicate that the velocity profile at each axial location not return to zero at the guidewire boundary (see Fig. 11). This indicates that the guidewire does not exhibit a no-slip boundary condition. There are several possible explanations for this observation. First, the material properties of the stainless steel guidewire (painted flat black to limit reflection of light) are different than that of the acrylic, artery wall. Therefore, the two different boundaries may demonstrate different behavior in their interaction with the experimental fluid due to an element of surface roughness.

Because the paint was applied by hand, it cannot be assumed that the paint itself is uniform in distribution across the entire face of the central annulus. The variation in paint thickness could provide an element of roughness to the surface area of the central annulus. Zhu and Granick (Zhu and Granick, 2002) have demonstrated that there are limits to the hydrodynamic no-slip boundary condition. The greater degree of roughness increases the threshold for slipping. In the case of particularly smooth surfaces, intermolecular forces dominate leading to a non no-slip boundary, or partial slip. This partial slip condition exists between the classical no slip condition as in Hagen-Poiseuille flow and the full slip condition which acts as if the boundary is simply not there. The experimental data indicate that neither the no slip nor full slip conditions are occurring in this case, but rather something in between.

Secondly, it is possible that there is a geometric significance with partial slip existing at the guidewire boundary. Given that the central annulus is quite small in comparison with the volume of fluid, it is possible that the effects of cohesion are stronger between the molecules of the fluid than the effects of adhesion between the fluid molecules and the painted stainless steel rod. The shear rate is also expected to be relatively large, which could cause slipping. In the case of the 20% stenosis, it appears that there is a constant slip velocity travelling alongside of the guidewire at all axial points. Figure 11 illustrates the velocity profiles within the 20 percent stenosis and

clearly shows that the boundary condition at the guidewire tends towards, but does not *fully go to zero velocity as it would with the artery* wall. The simulated results of this data are identical for all meshing configurations.

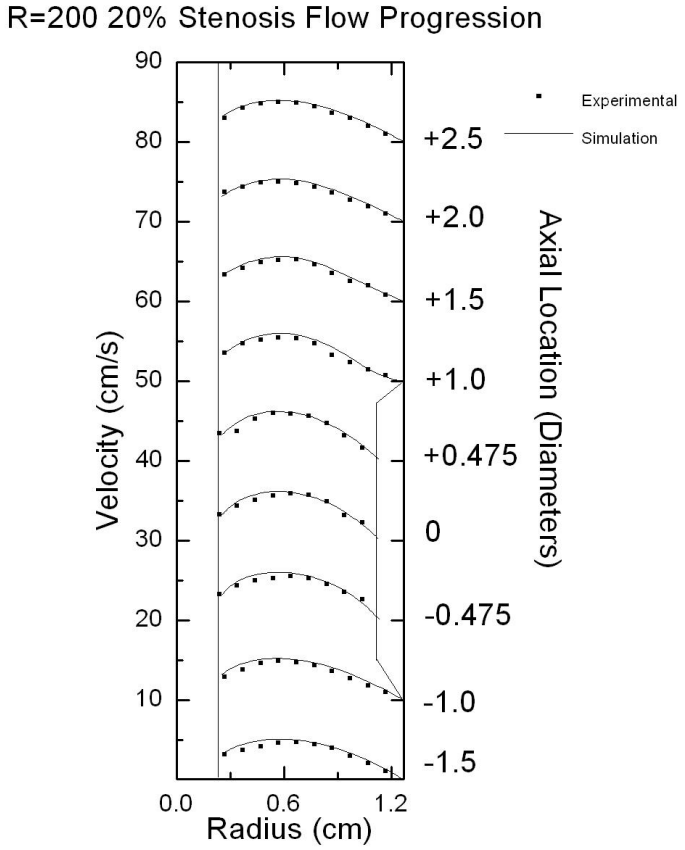

Figure 11. Flow progression of the 20% stenosis with guidewire. The guidewire is positioned on the left hand side of the graph with the stenosis oriented toward the right hand side. Velocity profiles again are separated by 10 cm/s intervals.

In order to fully capture the fluid behavior at the guidewire, a slip velocity had to be imparted to the overall average velocity, the dominating boundary condition. The same fluid properties as the case without the guidewire were used in terms of density, dynamic viscosity and all other physical boundaries. The guidewire was constructed to be perfectly straight and to run along the entire axis of symmetry from just downstream of the inlet to the outlet. A slip velocity equal to the average velocity was applied to the

guidewire boundary and stenosis face and artery wall were allowed to remain in the no slip boundary condition.

Results for the 20 % stenosis with the guidewire proved favorable with the slip velocity condition in place. The velocity curves agreed well with experimental data and the slip velocity at the guidewire appears to remain nearly constant and equivalent to the overall average velocity. There appears to be no slip occurring either at the artery wall or at the stenosis face according to both the experimental and simulated data.

B. 30% STENOSIS

1. No Guidewire Case

The 30 % stenosis parameters, with and without the guidewire, follows the same boundary conditions as the 20 % stenosis in terms of density, viscosity, and average velocity. The LDV samples taken outside of the stenosis itself are also the same ranging from 11.7 mm from the artery wall to 0. 7 mm from the center of the mock artery. Within the stenosis itself, one less data point per axial position was recorded due to the increased thickness of the stenosis. In this case, recorded measurements began at 9.6 mm from the tube center as opposed to 10.4 mm in the case of the 20 % stenosis.

Results of the 30 % stenosis closely matched that of experimental data (see Figure 12). The velocity profile reached its peak at the center of the artery and went to zero at the boundary. The significant difference between the 20 and 30 degree stenoses both in experimental and simulated data arose from the decrease in cross sectional area caused by the increase in the percentage size of the stenosis. It was expected by continuity that peak velocities within the tube would increase when compared with the peak velocities upstream of the stenosis while the average velocity between each axial location would be the same. Both experimental and simulation data confirm these hypotheses.

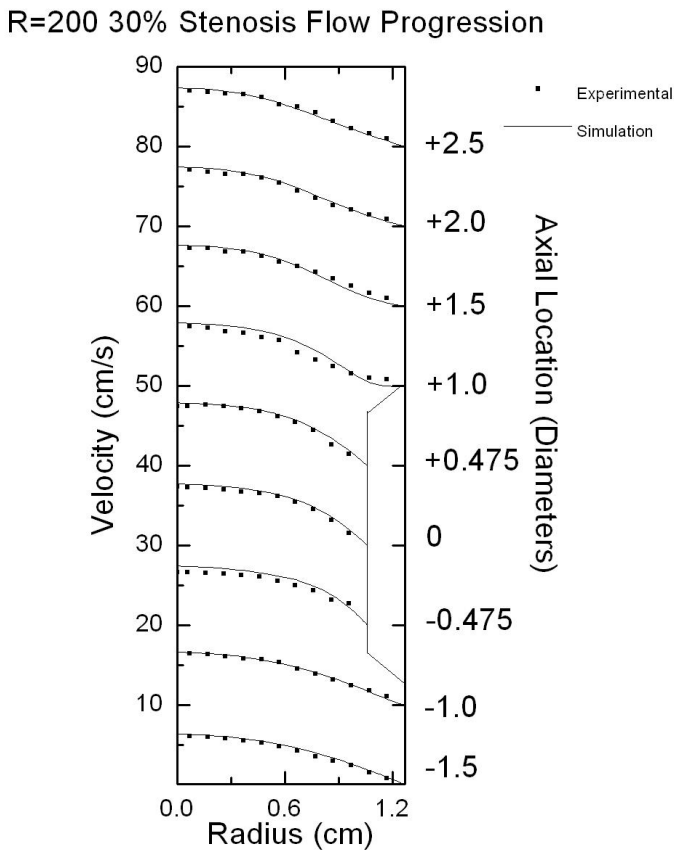

Figure 12. Flow progression of the 30 % stenosis, the fluid properties and initial conditions remain the same as the 20 % stenosis.

2. Guidewire Case

The 30 % stenosis with the guidewire present assumes the same boundary conditions as the 20 % with the guidewire installed. The partial slip applied to the guidewire was again the average velocity which was also equal to the experimental data point nearest to the guide wire at the -1.5D axial location. Flow progression generally represents experimental data though there appears to be indications of a new phenomenon occurring at the entrance to the stenosis (see Figure 12). The partial slip at the guidewire appears to be increasing when the flow enters the stenosis according to experimental data. In addition to the partial slip increase at the guidewire, the velocity profile is not represented by the Hagen-Poiseuille equation for laminar flow with a central annulus and is given by

$$u(r) = u_{\max} \cdot \left[R_2^{\,2} - r^2 + (R_2^{\,2} - R_1^{\,2}) \frac{\log\left(\frac{r}{R_2}\right)}{\log\left(\frac{R_2}{R_1}\right)} \right], \tag{4}$$

where u(r) is the axial velocity as a function of radius in m/s, u_{max} is the peak velocity in m/s, R_2 is the radius of the external duct in m, and R_1 is the radius of the central annulus (Landau and Lifshitz, 1987). The lamina away from the center of the flow have a higher magnitude that is more proportional to the peak velocity. In short, instead of a parabola with a sharp slope tending to zero at the boundaries, there is the onset of a more plateaued parabola that shows a smaller gradient between the peak velocity of the fastest lamina and the slower lamina toward the boundaries. Figure 13 shows the flow progression of the 30% stenosis at the 9 different axial locations. The -0.475D location clearly shows a broadening of the velocity profile when compared to the two other axial locations within the stenosis. The red line Figure 13 shows the simulation velocity profile at 0.705 diameters upstream of stenosis center. This is essentially the stenosis entrance where the flow first encounters the level face of the stenosis. At this location, simulated data closely resembles experimental data further downstream.

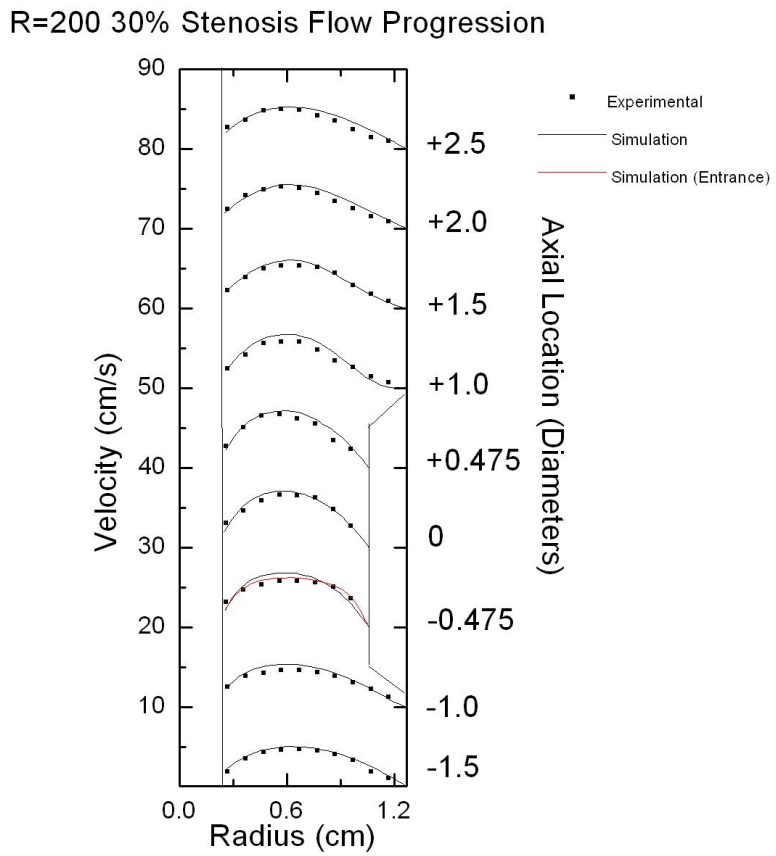

Figure 13. Flow progression of the 30 % stenosis, the red curve is the simulation flow profile at the entrance of the stenosis compared with 0.475 diameters upstream of mid-stenosis.

C. 40% STENOSIS

1. No Guidewire Case

From experimental data, the 40 % stenosis has the same fluid properties in terms of density, dynamic viscosity, and average velocity as the 20 and 30 % stenoses. The simulation boundary conditions, therefore, were left unchanged from previous studies. The sole change to the simulation set up came from replacing the 30 % stenosis with a 40% stenosis with a thickness of 2.9 mm. Data points outside of the stenosis retained the 1 mm interval between 11.7 mm from the center of the artery to 0.7 mm from the center of the artery.

Figure 14 shows the flow progression of the 40% stenosis from 1.5 diameters upstream of stenosis center to 2.5 diameters downstream of stenosis center. Of note, there appears to be the onset of a recirculation zone directly downstream of the stenosis at the +1.0D location. The onset of this recirculation (or backflow) is the result of an adverse pressure gradient from the stenosis and can be viewed as a nozzle-diffuser configuration with a high angle diffuser (White, 2002). The increasing cross sectional area at axial points downstream of the stenosis exit produces low velocity and increasing pressure where the growth of the boundary layer causes a point of inflection away from the artery wall. Additionally, this negative velocity region directly adjacent to the artery wall is a direct result of continuity through the increase of the peak velocity within the stenosis region. Despite this recirculation zone, velocity tends still tends toward zero at the artery wall.

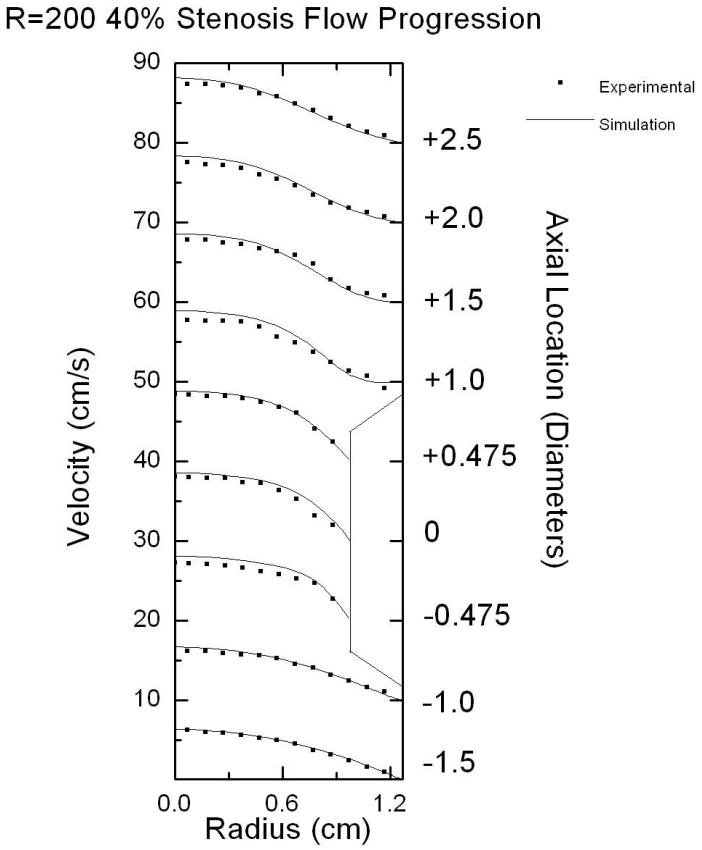

Figure 14. Flow progression of the 40% stenosis, experimental and simulation data show the onset of recirculation 1.0 diameters downstream of the stenosis center.

Also of note, there appears to be a continuation of the trend of a transient state (in terms of axial location) occurring at the entrance of the stenosis. While simulation data have a zero boundary velocity at the face of the stenosis, laboratory data show a possible slip velocity occurring at the stenosis entrance before gradually resuming a no slip boundary condition by the +0.475D axial location. While there is a radial component of velocity occurring at this location, the LDV collected only the axial component of velocity. The possibility of a slip velocity boundary is further supported by the fact in the simulation there is a greater peak velocity occurring towards the center of the artery with the boundary velocity dropping to zero. The experimental data, however, show a lower velocity occurring towards the center of the artery but even a small non-zero slip velocity would account for the change in the velocity magnitude towards the center due to the large change in area of the lamina from the center to the stenosis face.

2. Guidewire Case

As in the case of the 20 and 30 % stenoses, the slip velocity applied to the guidewire for the 40 % stenosis was set equal to the average velocity of the flow. The fluid parameters remained the same as in the case of previous stenoses. The slip velocity condition applied at the guidewire remains an appropriate approximation outside of the confines of the stenosis. Within the stenosis, there appears to be a greater slip velocity occurring at the guidewire as well as a non-zero boundary velocity at the stenosis face. Figure 15 shows the progression of the flow through the 40% stenosis. The simulated entrance profile does not make the same appropriate fit as in the case of the 30% stenosis with the guidewire, which is expected due to the greater flow rate caused by the stenosis. There is a notable increase in the slip velocity at the guidewire. Like the 30 % stenosis with the guidewire, there appears to be a transition region at the stenosis face where the slip velocity decreases from a non-zero value to a no slip condition appearing once flow passes through the center of the stenosis.

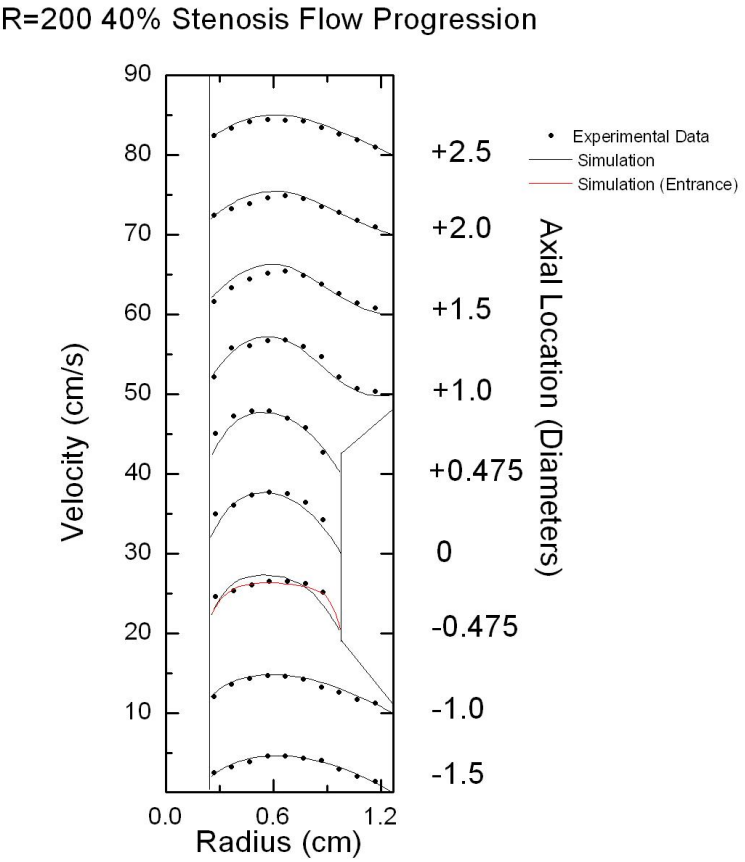

Figure 15. Flow progression of the 40% stenosis with guidewire. Note the increase of the slip velocity at both boundaries within the stenosis itself. The red curve represents the flow profile directly at the stenosis entrance vice 0.475 diameters upstream

D. 60% STENOSIS

1. No Guidewire Case

The 60 % stenosis experimental setup varies from its predecessors in that the basic properties of the test fluid change. This change is manifested through a change in the density and dynamic viscosity which, in turn, causes a change in average velocity applied. The density increased from 1115.5 kg/m3 to 1133.2 kg/m3 and the dynamic viscosity increased from 4.4745 to 6.2536 mPa*s. While average velocity boundary conditions were still applied from the one half of the maximum velocity in the no guidewire case [equation (2)], calculations were also conducted in accordance with

equation (1) to verify consistency. As a result the average velocity increased from 3.1584 cm/s to 4.3453 cm/s. This average velocity was set equal to the inlet average velocity in the model.

Outside of the stenosis, the axial and radial locations of measurement were different from previous setups. Instead of measuring axial velocities at 1 mm intervals from the artery wall, the initial measurement was taken at 0.6 mm from the artery wall and at 1mm intervals thereafter with the most central of data points taken at 0.1 mm from the artery center. Within the stenosis, the increasingly constricted nature of the flow reduced the number of data points to eight ranging from 0.6 mm from the stenosis face to 0.01 mm from the artery center. A 60% stenosis yielded a stenosis thickness of 4.7 mm thus making the outermost data collection point occurring at 7.4 mm from tube center.

Figure 16 shows the flow progression through the 60% stenosis without the guidewire. The velocity profiles upstream of the stenosis show good agreement with experimental data as well as the velocity profiles downstream of stenosis center. Much like the 40% stenosis case without the guidewire, there is a region of recirculation downstream of the stenosis itself. However, this region of recirculation extends far beyond the one diameter downstream point. For the 60% stenosis, recirculation occurs until approximately two diameters downstream of stenosis center.

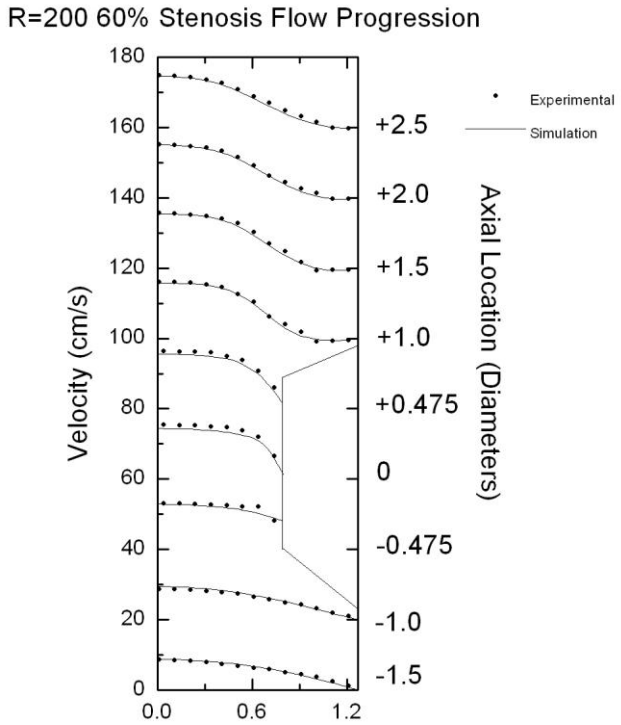

Figure 16. Flow progression of the 60% stenosis without guidewire. In this case, the velocity profiles are set at 20 cm/s intervals to allow from greater clarity due to their increased magnitude when compared with smaller grade stenoses.

Within the stenosis itself, there appears to be a pattern emerging for the slip velocity at the stenosis face. While the slip velocity is nearly half the magnitude of the maximum velocity at the stenosis entrance, this trends toward a no slip condition by the time the flow is past stenosis center. In addition, the maximum magnitude of the velocity at the central lamina is higher in simulated data than experimental data when the no-slip boundary condition is applied. A slip velocity parameter was introduced at the stenosis face to account this region and is shown in Figure 16. The slip velocity parameter applied was a linear equation to account for the decrease in boundary velocity as the flow progressed through the stenosis. It was implemented by interpolating the experimental data to create a virtual boundary velocity that decays to zero as the flow progresses downstream. With this method, simulation data show much greater agreement both within and downstream of the stenosis, the peak velocity is lowered to show more agreement with experimental data, and the unique behavior at the stenosis entrance is more accurately modeled.

2. Guidewire Case

The guidewire case for the 60 % stenosis clearly demonstrates new effects due to the higher degree of flow obstruction. Compared with the previous guidewire cases where there appears to be a constant non-zero slip velocity, the 60 % stenosis shows different effects in experimental data (see Figure 17). Upstream of the stenosis, the experimental slip velocity at the guidewire appears to be on the same order as the average velocity, much like the lesser stenoses. However, upon stenosis entrance, the slip velocity at the guidewire increases to approximately three times the upstream magnitude. Upon exiting the stenosis, the slip velocity begins to decrease, still above the average velocity but trending toward it. Velocity at the boundary is also occurring at the stenosis face. This effect is similar to the effects seen in the 60 % stenosis without the guidewire. The boundary velocity increases rapidly at the stenosis entrance and then decreases as it progresses axially downstream. The axial location within the stenosis does have a positive, non-zero boundary velocity unlike previous experimental setups where the velocity is zero and a no-slip condition is either maintained or established.

A similar method for modeling the behavior within the stenosis was developed as was the case for the 60 % stenosis without the guidewire. Experimental data was interpolated to account for a slip velocity at the stenosis face that decays toward zero as flow is established within the stenosis. Additionally, a second boundary slip velocity was necessitated at the guidewire. Given that the central annulus boundary velocity did not remain on the same order as the average velocity, a linear equation was applied to the length of central annulus within the vicinity of the stenosis.

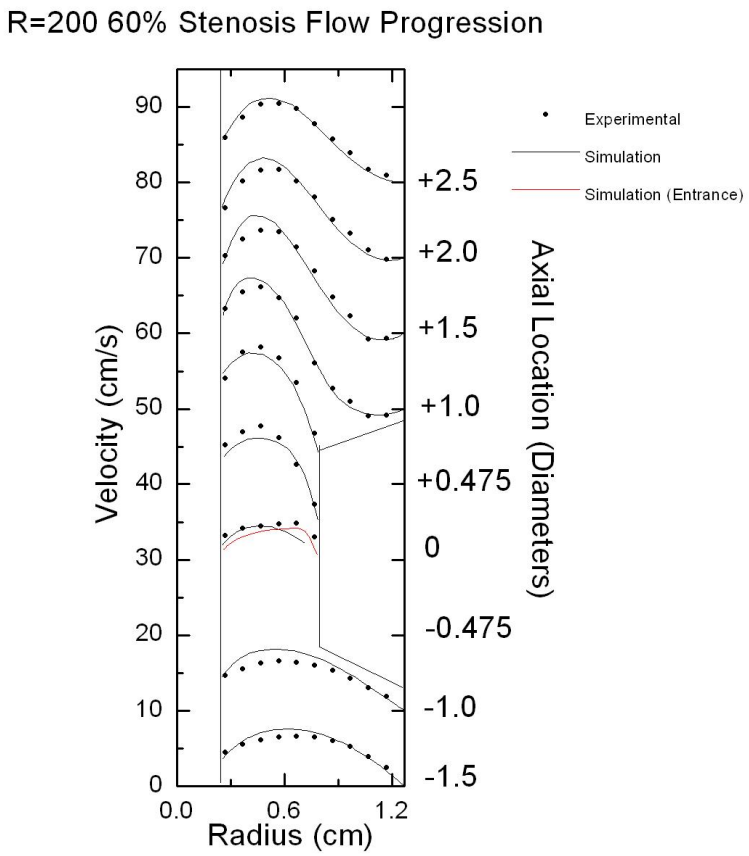

Figure 17. Flow profile of the 60% stenosis with guidewire. The red curve represents simulated data occuring at the stenosis entrance vice the 0.475 diameter upstream axial lcoation.

E. 75% STENOSIS

1. No Guidewire Case

The 75 % stenosis utilized new fluid parameters from the previous experimental sets. Periodic purging and cleaning of the head tank necessitated fluid replacement. As a result, the water and glycerol combination was not always mixed to the same proportions. In the case of the 75 % stenosis, the mixture produced a density of 1167 Kg/m^3 and a viscosity of 11.833 mPa·s. Observed maximum velocity upstream of the stenosis was 18.5 cm/s, and the average velocity was calculated to be 9.25 cm/s for the no guidewire case.

Data collection outside of the stenosis reverted to the method for the 20, 30, and 40 % stenoses with the outermost data point being 1 mm from the artery wall and the innermost data point being 0.7 mm from artery center. Within the stenosis, greater resolution of the velocity profile was produced by decreasing the radial distance between measurements to 0.5 mm. The 75 % stenosis had a thickness of 6.35 mm thus giving the artery a radius of 6.35 mm as well. Figure 18 shows the progression.

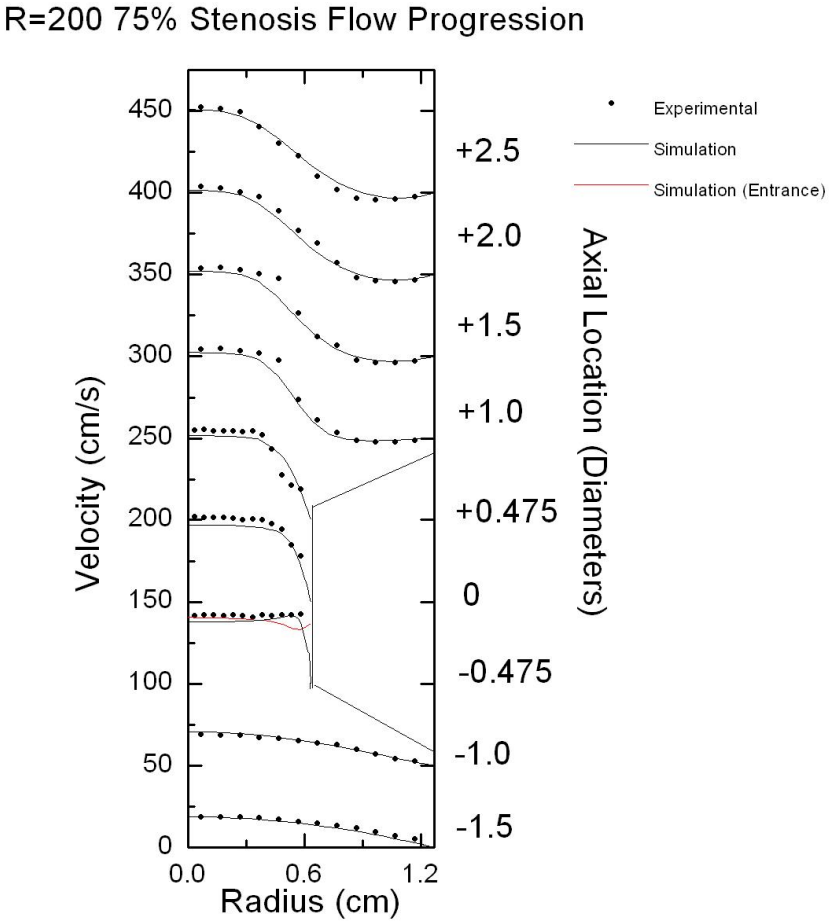

Figure 18. Flow progression of the 75% stenosis Note the broad, non-parabolic profile at the -0.475D axial location. The red curve represents simulation data from the stenosis entrance vice the 0.475 diameter upstream axial location.

The 75 % stenosis experimental data confirm the drastic change in the velocity profile as the flow enters the stenosis. In this case, the velocity profile at the stenosis

entrance is nearly purely horizontal and approximately four times the magnitude of the average velocity. Additionally, the slip velocity occurring along the stenosis face does not go completely to zero, even at the stenosis exit as was the case with the lower grade stenoses. The flow profiles beyond the stenosis show a recirculation region that extends beyond the last axial data point. As was the case of the 60 % stenosis without the guidewire, a slip velocity boundary condition was imposed at the stenosis face and shows greater agreement in both magnitude and profile shape as experimental data.

2. Guidewire Case

When the guidewire is applied to the 75 % stenosis similar effects are found as in the case of the 60 % stenosis with the guidewire. For this experimental setup, 3 separate fluids were utilized as shown in Figure 19. The three separate fluids were caused by the periodic requirement to clean and purge the head tank. The fluid upstream of the stenosis, shows predicted behavior with the slip velocity at the guidewire approximately equal to the overall average velocity of the two different fluids used.

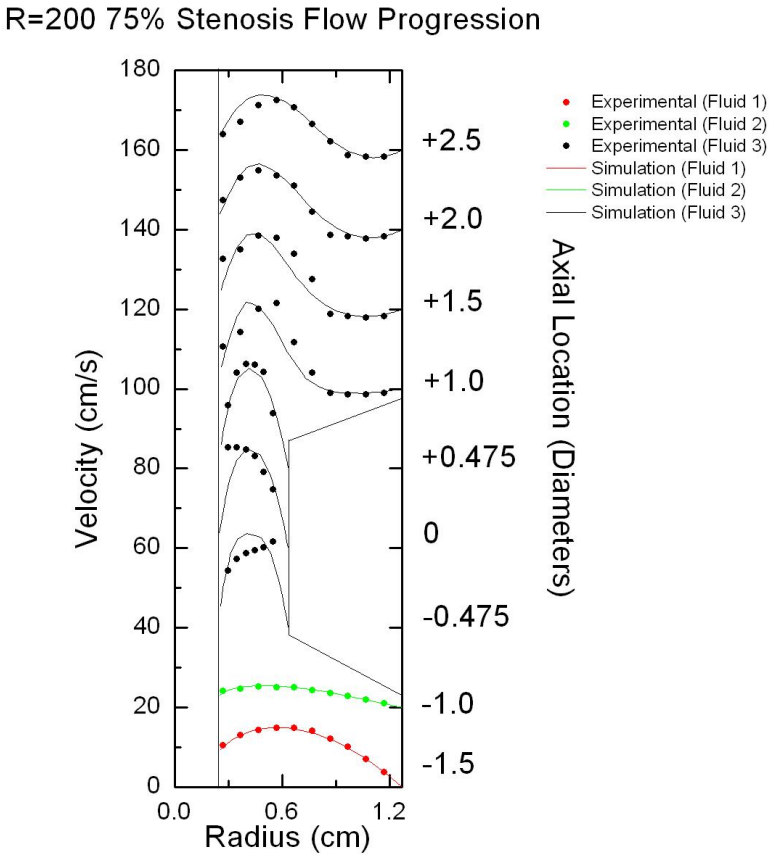

Figure 19. Flow progression of the 75 % stenosis. The three different fluids are denoted by the change in color. Note the appreciable change of the shape of the profile as the flow progresses through the stenosis.

Downstream of the stenosis, the trend continues where initial guidewire velocity is much higher than the average velocity but progresses back to the average velocity as it travels axially downstream. Within the stenosis itself, there is a new, unique behavior.

The profile appears to change rapidly as a function of axial distance. At the stenosis entrance, it appears as if there is a no slip condition acting at the stenosis face. This is shown by the lower magnitude velocity occurring at the guidewire and the maximum magnitude velocity occurring toward the boundary. As the fluid travels to the middle of the stenosis, it appears as though there is a total slip condition at the guidewire, while the stenosis face appears to have a no slip condition. At the exit of the stenosis, the flow appears approximately consistent with the model.

F. 90% STENOSIS

1. No Guidewire Case

The 90 % stenosis case without the guidewire was conducted with two separate experimental fluids. The flow progression in Figure 20 shows the rapid increase in velocity magnitude at the stenosis entrance. When compared with the no guidewire case for the 75 % stenosis, the velocity profile no longer appears to be uniform at the stenosis entrance but rather there is a much greater magnitude of velocity toward the stenosis face. This can be qualitatively accounted for due to the large volumetric flow from the radially outward portion of the cylinder being channeled into a very narrow area. As the flow progresses, the velocity profile returns to apparent no slip conditions at the stenosis face as denoted by the profiles at the 0D and +0.475D locations.

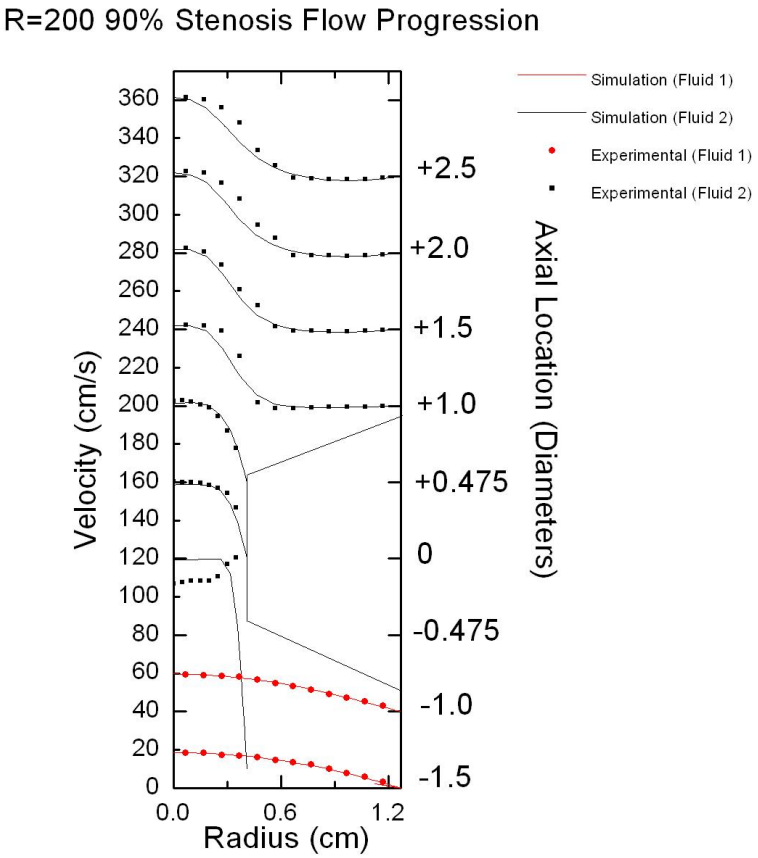

Figure 20. Flow profile of the 90% stenosis without guidewire. Fluid 1 is denoted in red and Fluid 2 is denoted in black.

Downstream of the stenosis, there is a larger recirculation region than with the smaller grade stenoses. The increased velocity region is confined radially to a region comparable with the size of the stenosis. Experimental data show an expansion of this increased velocity region much closer to the stenosis exit than simulation data show.

2. Guidewire Case

The guidewire case for the 90 % stenosis shows a new phenomenon Figure 21. It appears that there may be a turbulent condition downstream of the stenosis. The simulation, with its laminar flow assumption, would compute only for a Reynolds number of 200. Clearly, a threshold was crossed when Reynolds numbers of 300 and 400

were attempted in simulation. Figures 21, 22, and 23 show the velocity profiles. There is still agreement with the upstream portion of the flow for Reynolds numbers of 200, 300, and 400.

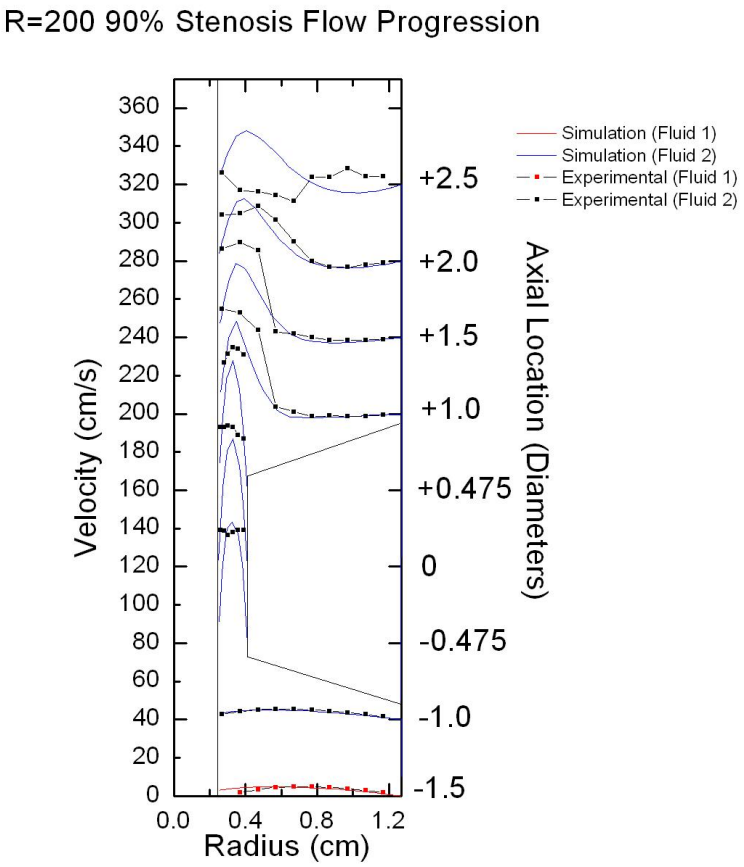

Figure 21. The 90% Stenosis with the guidewire for Re=200 when compared with the computer model. Note the atypical behavior at the +2.5D location.

As the flow progresses into the stenosis, that agreement rapidly falls off. As the flow leaves the stenosis, there appears to be an increased velocity profile toward the center of the tube for the following three axial locations. At the fourth axial location downstream, +2.5D, there is no semblance of organized, laminar flow as demonstrated by the much higher velocity magnitude toward the artery wall when compared with the flow toward the guidewire.

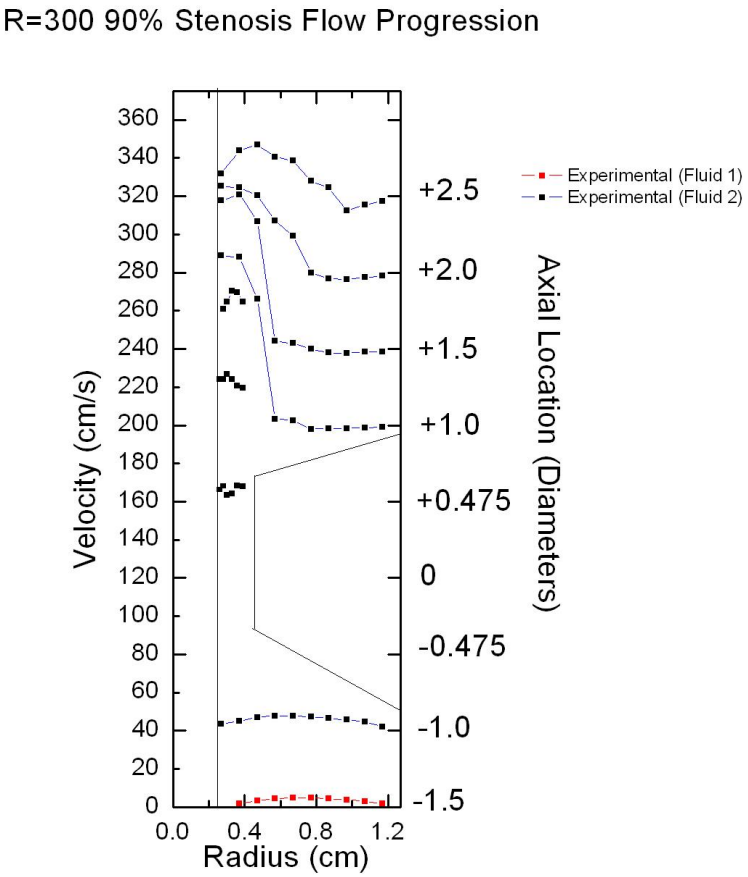

Figure 22. The 90% stenosis with the guidewire for Re=300. Note the large changes in peak velocity near the radial center of the artery. Experimental data only.

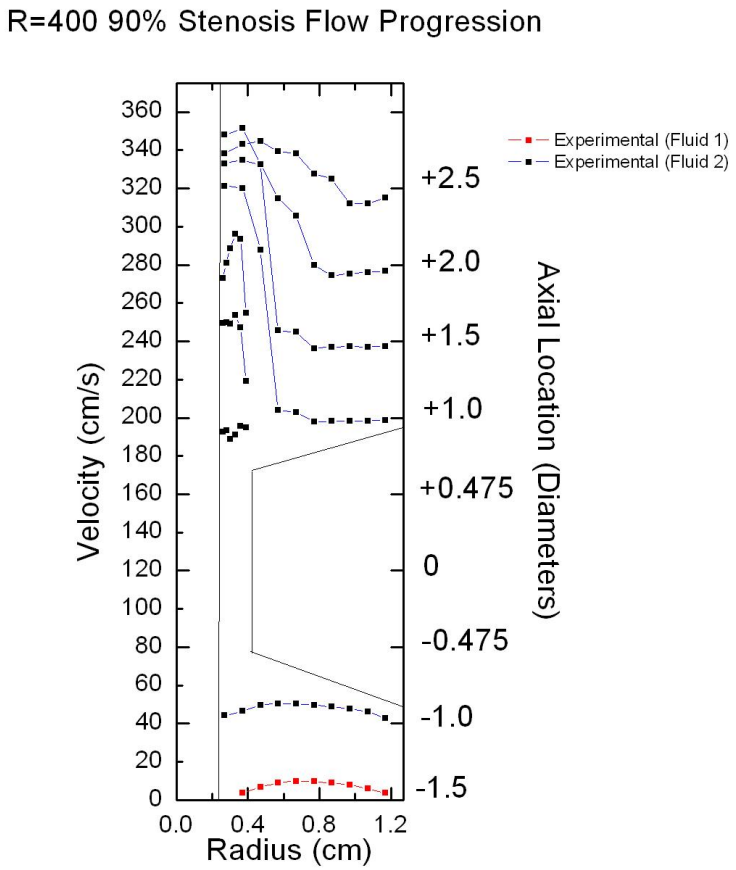

Figure 23. The 90% stenosis with guidewire for Re=400. Note the difference between the shape of the profiles at the +0.475D axial location when compared with Re=300. The peak velocity at Re=400 appears to be closer to the face of the stenosis while closer to the center of the channel at Re=300.

At Reynolds numbers of 300 and 400, only the experimental data are shown for comparison purposes. The higher Reynolds numbers also show similar velocity profiles upstream and within the stenosis, along with a sharp decrease in velocity magnitude at 2.5 diameters downstream. The large discrepancies between each of the downstream axial locations suggests that the linear relationship between Reynolds number and flow profile no longer exists at the 90 % stenosis with the guidewire.

THIS PAGE INTENTIONALLY LEFT BLANK

V. CONCLUSIONS AND FUTURE WORK

The simulations run via COMSOL multiphysics largely appear to have accurately depicted the in vitro experiment conducted. This is especially apparent in the lower grade stenoses (approximately 40 percent and below). The model is not without its limitations however. The guidewire in and of itself, presents a unique challenge that is not well understood. Applying a moving wall boundary condition allowed for simulation results comparable to experimental data in many cases but did not totally account for the change in the velocity profile within the stenosis itself.

The rapid rise in velocity at the stenosis entrance also provided a challenge for the computer model. The boundary conditions initially dictated that the fluid velocity at the boundary would always be zero. COMSOL's adherence to such a condition showed clear disagreement with experimental data. While in all experimental data cases, the boundary velocity at the stenosis face does eventually tend towards zero, the simulations show a much faster transition to that point and are only solved through modifying a linear slip velocity condition that is dependent on the severity of the restriction.

While it is evident that there remains issues to be resolved at the higher grade stenoses, it is encouraging that the lower grade stenosis simulations appear to show excellent agreement with experimental data. Given that stent installation either occurs when a lower grade stenosis is present or forcibly decreases the constriction of the flow by expanding the artery, the 20% to 40% stenoses would remain prime candidates for active monitoring.

Additionally, periodic routine use of a potential cardiovascular MEMs device would not occur while a guidewire was in place, thus eliminating some of the ambiguity associated with a high boundary velocity along a guidewire. In essence, blood flow monitoring would occur in a less diseased and a less complex operating environment than the simulations attempted to duplicate.

There are three main focus areas for future work in order to develop a viable MEMS device to serve as an arterial stent. First, a non-stationary flow must be analyzed.

Within its laminar flow module, COMSOL provides a means to develop pulsatile flow. This can be done by scaling up the current model and implementing a periodic flow condition that would represent the human cardiovascular system's systolic and diastolic blood pressure. Study in this area would necessitate a non-stationary study that greatly increases the complexity and solution time but would provide a possible dynamic environment where a MEMS type sensor could operate. The fluctuation in pressure would also dictate a fluctuation in the velocity near such a device (in this case, the channel wall) which would in turn cause a change in the force on the sensor. If the sensor was a piezoresistive material, this change in force would cause a change in voltage readout that would provide an indication of how the flow properties are changing over time.

In addition to studying a more dynamic and time dependent environment, the flow properties of a non-Newtonian fluid must be observed under similar conditions. Blood itself is a non-Newtonian fluid and has different behaviors and properties than the distilled water and glycerol combination in both the previous experiments as well as the simulations. In order to determine the appropriateness of the current model, simulation with a non-Newtonian fluid must be conducted in order to compare results and determine further viability.

The third main focus area of future work is development of the MEMs device itself. This would include, but not be limited to, design and testing of a MEMs pressure or velocity sensor through computer simulation modeling. Given the inherent MEMS and fluid dynamic modules within COMSOL, it remains the logical choice for future work in MEMS simulations. The software enables the user to change the geometry, dimension, and materials in order to determine the optimal design for future laboratory testing.

In addition to the areas of future research and study, analysis and simulation have revealed the need for greater study and understanding within the field of fluid dynamics. For example, the phenomenon associated with the boundary velocity at the guidewire is not well understood and is merely approximated with a slip velocity boundary condition in order to enable the simulation model agree with the experimental data. It is not well

understood whether that occurrence at the boundary is associated with some degree of slipping, some type of turbulent boundary layer caused by a very high shear rate, or merely a function of geometry.

Additionally, the abnormal boundary conditions at the face of the stenosis for the higher grade stenoses (60% and above) must also be understood with greater clarity. Experimental data clearly show a very high relative velocity near the stenosis face when compared with the average velocity or the simulation when using the no slip boundary condition. It is possible that this phenomenon at the boundary is not associated with the phenomenon occurring at the guidewire given that it is present even in the cases without the guidewire. Additional possibilities include a turbulent boundary layer associated with a large volumetric flow rate proceeding through a very small channel as well as a possible slip condition imposed by the geometry and material makeup of the model stenoses.

THIS PAGE INTENTIONALLY LEFT BLANK

LIST OF REFERENCES

Aiyar, A., Song, C., Kim, S., &Allen, M., (2009, July) An all-polymer airflow sensor using a piezoresistive composite elastomer, *Smart Materials and Structures* 18, 19.

DeMaria, A., N., Baxa, J., B., Ben-Yehuda, O., Feld, G., K., Greenberg, B., Hall, J., Hlatley, M., Lew, W., Y., W., Lima, J., A., Maisel, A., S., Narayan, S., M., Nissen, S., Sahn, D., J., &Tsimikas, S., (2011, July) Highlights of the year in JACC 2010, *Journal of the American College of Cardiology*, 57(4), 480–541.

Denardo, S., Talbot, L., Hargrave, V., Fitzgerald, P., Selfrdige, A., & Yock, P., (1994, July) Analysis of pulsed wave doppler ultrasound spectra obtained from a model intracoronary catheter, *IEEE Transactions on Biomedical Engineering*, 41(7), 635–648.

Denardo S., Talbot, L., Hargrave, V., Selfridge, A., Ports, T., &Yock, P., (1997, February) Accuracy of doppler catheter measurements: effects of inhomogeneous beam power distribution on mean and peak velocity, *Journal of the American College of Cardiology* 29(2), 283-292.

Garg, S., & Serruys, P., W., (2010, December) Coronary stents: current status, *Journal of the American College of Cardiology*, 56(10), S1-S42.

Keikhosravy, K., Zargaran-Yazd, A., & Mirabbasi, S., (2012) On the use of smart stents for monitoring in-stent restenosis. *In Procedings of 34th International Conference of the IEEE EMBS* (pp. 3231-3234).San Diego, California,.

Landau, L.D.& Lifshitz, E.M., (1987). *Fluid mechanics*, (2nd ed.) New York: Butterworth-Heinemann.

Takhata, K., Gianchandani, Y., & Wise, K. (2006, October). Micromachined antenna stents and cuffs for monitoring intraliminal pressure and flow, *Journal of Microelectromechanical Systems*, 5, 1289–1298.

White, F., (2003). *Fluid mechanics*, (5th ed.) New York: McGraw Hill.

World Health Organization, (2013). *World health statistics 2013* Geneva: WHO Press.

Zhu, Y. &Granick, S., (2002, March) Limits of hydrodynamic no-slip boundary condition, *Physical Review Letters*,88(10), 106102-1–106102-4.

THIS PAGE INTENTIONALLY LEFT BLANK

INITIAL DISTRIBUTION LIST

1. Defense Technical Information Center
   Ft. Belvoir, Virginia

2. Dudley Knox Library
   Naval Postgraduate School
   Monterey, California